Potassium Currents in Freshly Dissociated Uterine Myocytes from Nonpregnant and Late-Pregnant Rats

S.Y. Wang, M. Yoshino, J.L. Sui, M. Wakui, P.N. Kao, and C.Y. Kao†

From the Department of Pharmacology, State University of New York Health Science Center, Brooklyn, New York 11203

ABSTRACT In freshly dissociated uterine myocytes, the outward current is carried by K^+ through channels highly selective for K^+. Typically, nonpregnant myocytes have rather noisy K^+ currents; half of them also have a fast-inactivating transient outward current (I_{TO}). In contrast, the current records are not noisy in late pregnant myocytes, and I_{TO} densities are low. The whole-cell I_K of nonpregnant myocytes respond strongly to changes in $[Ca^{2+}]_o$ or changes in $[Ca^{2+}]_i$ caused by photolysis of caged Ca^{2+} compounds, nitr 5 or DM-nitrophene, but that of late-pregnant myocytes respond weakly or not at all. The Ca^{2+} insensitivity of the latter is present before any exposure to dissociating enzymes. By holding at −80, −40, or 0 mV and digital subtractions, the whole-cell I_K of each type of myocyte can be separated into one noninactivating and two inactivating components with half-inactivation at approximately −61 and −22 mV. The noninactivating components, which consist mainly of iberiotoxin-susceptible large-conductance Ca^{2+}-activated K^+ currents, are half-activated at 39 mV in nonpregnant myocytes, but at 63 mV in late-pregnant myocytes. In detached membrane patches from the latter, identified 139 pS, Ca^{2+}-sensitive K^+ channels also have a half-open probability at 68 mV, and are less sensitive to Ca^{2+} than similar channels in *taenia coli* myocytes. Ca^{2+}-activated K^+ currents, susceptible to tetraethylammonium, charybdotoxin, and iberiotoxin contribute 30–35% of the total I_K in nonpregnant myocytes, but <20% in late-pregnant myocytes. Dendrotoxin-susceptible, small-conductance delayed rectifier currents are not seen in nonpregnant myocytes, but contribute ~20% of total I_K in late-pregnant myocytes. Thus, in late-pregnancy, myometrial excitability is increased by changes in K^+ currents that include a suppression of the I_{TO}, a redistribution of I_K expression from large-conductance Ca^{2+}-activated channels to smaller-conductance delayed rectifier channels, a lowered Ca^{2+} sensitivity, and a positive shift of the activation of some large-conductance Ca^{2+}-activated channels.

KEY WORDS: smooth muscle cells • uterine myocytes • K^+ channels • pregnancy • ovarian hormones

INTRODUCTION

Under influences of ovarian hormones and during pregnancy, ionic currents of uterine myocytes undergo some profound changes, such as the emergence of a high-affinity tetrodotoxin-sensitive Na^+ current, and its increasing density relative to a coexisting Ca^{2+} current as pregnancy progresses to term (Yoshino et al., 1997). Another striking change occurs in the outward current where a noisy Ca^{2+}-sensitive K^+ current, prominent in nonpregnant and early-pregnant myocytes, is largely replaced by a smooth Ca^{2+}-insensitive current in late-pregnant myocytes (Kao et al., 1989; Wang et al., 1996). Such a transformation could be due to changes in the properties of some K^+ channels, to changes in the relative roles of different types of K^+ channels, or combinations of these possibilities.

Multiple types of K^+ currents have been known for some time (see Hille, 1992), and more than a score of different K^+ channels have been identified by recombinant DNA methods (Chandy and Gutman, 1995; Jan and Jan, 1997). A chief aim of this work is to determine the contributions of different K^+ channels to the total outward current of uterine myocytes at different stages of pregnancy in the rat. To this end, we separated the whole-cell K^+ currents of nonpregnant and late-pregnant myocytes into components containing fewer overlapping currents, and studied their kinetic and steady state gating properties, responsiveness to intra- and extracellular Ca^{2+}, and susceptibility to selective blocking agents. We also examined single-channel properties of the large-conductance Ca^{2+}-activated K^+ channel and related them to whole-cell K^+ currents. We find that during pregnancy the expression of the outward current shifts from these channels to other types of K^+ channel, and that the shift together with other changes in K^+ currents can increase myometrial excitability. Preliminary accounts of some of this work have been presented (Suput et al., 1989; Kao et al., 1989; Yoshino et al., 1989, 1997; Wang et al., 1996).

METHODS

Multicellular Preparations

Myometrial strips were taken from pregnant rats of known gestation. Small strands of the longitudinal myometrium were studied in a double sucrose-gap chamber, where the region ("node") un-

†Dr. C.Y. Kao died on May 26, 1998.

Address correspondence to Peter N. Kao, M.D., Ph.D., Pulmonary and Critical Care Medicine, Stanford University Medical Center, Stanford, CA 94305-5236. Fax: 650-725-5489; E-mail: peterkao@leland. stanford.edu

J. Gen. Physiol. © The Rockefeller University Press • 0022-1295/98/12/737/20 $2.00
Volume 112 December 1998 737–756
http://www.jgp.org

der current or voltage clamp averaged 65 μm, with total capacitance of ~100 pF (Kao and McCullough, 1975). The nodes, formed by interfaces of flowing sucrose and Krebs solution, are now known to contain ~1,000 myocytes (Yoshino et al., 1997). Aside from being dissected free from the uterus and subjected to two cuffs of high-resistance isotonic sucrose solution, these strands were not exposed to any enzymes or mechanical disruptions, nor were their cell interior exposed to any artificial Ca^{2+} buffers.

Dissociated Myocytes and Single-Channels Studies

Myocytes were obtained from nonpregnant (estrus phase) and late-pregnant (17–21 d) rat uteri (see details in Yoshino et al., 1997). The main differences for the present study lie in the use of some agents and solutions for specific projects to sort out different types of K^+ channels. They are 4-aminopyridine (Hach Chemical Co., Ames, IA), charybdotoxin (Calbiochem Corp., San Diego, CA), iberiotoxin (Peptides International, Louisville, KY), dendrotoxin (Calbiochem Corp.), apamin (ICN Biochemicals Inc., Costa Mesa, CA), mast-cell degranulating peptide (Peninsula Laboratory, Belmont, CA), nitr-5 and DM-nitrophene (Calbiochem Corp.).

In experiments to identify charge carriers of the outward current, the bath solution contained (mM): 140 KCl, 0.6 EGTA, and 0.01 $CaCl_2$, pH 7.3, with a maximum free $[Ca^{2+}]$ of 7 nM. To test the role of Cl^- in the outward current, the 140 mM KCl was replaced with 100 mM K_2SO_4, the two being equiosmolar as determined by osmometry.

Photolysis of Caged Ca^{2+} Compounds

These experiments aimed at increasing intracellular Ca^{2+} ($[Ca^{2+}]_i$) directly to see how the outward current might be affected. An inverted microscope with an epifluorescence attachment was used (Diaphot; Nikon Inc., Melville, NY). The photolabile caged Ca^{2+} compound, nitr 5 (Gurney et al., 1987), was introduced into the cell by diffusion from the pipette, which contained 2 mM nitr 5, 1 mM Ca^{2+}, and 140 mM K^+. Filtered light of 330–380 nm was focused onto the myocyte through a 40 × "Fluor" objective (Nikon Inc.) that had a numerical aperture of 0.85 and transmittance to 340 nm. Exposure was controlled by a shutter (Vincent Associates, Rochester, NY). The photoenergy was insufficient to produce "flash" photolysis, and exposures lasted 100–800 ms. Such long exposures did not interfere with our interest in steady state effects. DM-nitrophene, another caged Ca^{2+} compound (Kaplan, 1990) was used in a generally similar way.

The concentration of Ca^{2+} attained on photolysis of nitr 5-Ca was estimated under simulated conditions. Ca^{2+}-selective microelectrodes were made by introducing a neutral Ca^{2+}-selective ion exchange resin (ETH 1001; World Precision Instruments, New Haven, CT; Amman, 1986) into the first 200 μm of previously silanized microelectrodes with tip openings of 1–1.5 μm. In standard solutions of pCa 7 to 3, the response of the microelectrodes was linear from pCa 6.5 to 3, with a slope of 29 mV/pCa U. Between pCa 7 and 6.5, the slope was 20 mV. To estimate the $[Ca^{2+}]$ released by photolysis, a Ca^{2+} microelectrode and a reference electrode were placed in a 10-μl droplet of the pipette solution within the microscope field. The droplet was exposed to UV light for 10–800 ms. The response of the microelectrode stabilized within 26 to 40 s. The basal $[Ca^{2+}]$ before UV exposure was 0.4–0.47 μM (six trials; see also Gurney et al., 1987). Upon irradiation, the increment of $[Ca^{2+}]$ was 0 μM for 10 ms, 1.8 μM for 100 ms, 8.2 μM for 400 ms, 14.6 μM for 800 ms, and 44 μM on continuous exposure. The true $[Ca^{2+}]_i$ attained must be less because of the presence of additional Ca^{2+}-buffering system in the cell.

Single-Channel Studies

Detached inside-out patches were used because $[Ca^{2+}]_i$ could be confidently controlled and readily altered. Openings identified as K^+ channels were surveyed, and large-conductance Ca^{2+}-activated K^+ channels were selected for study. The methods used were similar to those described for other smooth myocytes (*taenia coli*, Hu et al. 1989*a*,*b*; Fan et al., 1993; ureter, Sui and Kao, 1997). Separated or overlapped openings of different amplitudes were considered as different channels rather than subconductance levels of the same channel, because the larger (assumed full) and smaller (assumed sublevels) openings were random and unrelated. Overlapped openings of the same amplitude were assumed to be of the same channel type. In each condition, 1,000–10,000 channel events were collected. The records were examined for the highest overlap level in the more active recordings taken at highly positive voltages (80 mV), and in high $[Ca^{2+}]$ (pCa 6). Relative activities of different types of channels were determined by analyzing all channel openings during a recording period in 0.1 pA bins every 150–200 μs. The number of channels in a patch was derived from the highest overlapped opening level; and the averaged single channel activities were calculated for all channels. The average open-probability (P_o) for patches with multiple channels of the same amplitude was estimated when the number of channels in the patch could be reasonably determined. When the number of channels was uncertain, the open-probability was shown as nP_o.

In RESULTS, averaged values are given as means ± SEM. Significance of differences were evaluated by Student's *t* test in either the paired or unpaired form, as appropriate.

RESULTS

CHARGE CARRIER OF THE OUTWARD CURRENT

In the myometrium, at the usual resting potential of approximately −50 mV, E_{Cl} is approximately −20 mV (Kao and Siegman, 1963); in principle, Cl^- influx during depolarization could contribute to the whole-cell outward current (Parkington and Coleman, 1990). The charge carrier is identified as follows: when uterine myocytes were immersed in 140 mM KCl or 100 mM K_2SO_4 (pCa = 8.13), the resting potential was close to 0. When they were held to −80 mV, and then depolarized, the steady state current (at 0.5 s) was inward at negative voltages and outward at positive voltages. This phenomenon was confirmed in nine myocytes, regardless of whether Cl^- or SO_4^{2-} was the anion. The 0-mV reversal potential observed under asymmetric chloride concentrations indicates that potassium is the dominant charge carrier.

WHOLE-CELL K^+ CURRENTS OF UTERINE MYOCYTES AND THEIR RESPONSES TO CA^{2+}

The outward currents of freshly dissociated nonpregnant and late pregnant uterine myocytes are quite different with regard to time dependence, relative amplitudes, inherent noise, and calcium dependence. To delineate separate potassium channel contributions, it is necessary first to differentiate the general properties of the outward current in the nonpregnant and late-pregnant myocytes.

Nonpregnant Myocytes

In nonpregnant myocytes (Fig. 1, *A–C*), the outward currents first appeared at approximately −30 mV. At ~0 mV, they began to exhibit frequent large fluctuations (noisy) and distinct outward rectification. When elicited from a holding potential (HP)[1] of −80 mV, about half of the myocytes had an initial surge that peaked at 3.8 ± 0.5 ms (10 myocytes), and then fell in another few milliseconds to merge into a current that rose and declined more slowly (Fig. 1 *A*). The initial surge is due to a transient outward current (I_{TO}). In the other half of nonpregnant myocytes, no I_{TO} was present and the current rose gradually to reach a maximum at 24.8 ± 2.6 ms (10 myocytes). In both types of myocytes, the outward current decayed appreciably. In myocytes with an I_{TO}, the current was ~50% of the maximum by 235 ms (see current–voltage relations in Fig. 1 *C*) and ~20% by 1.1 s (not shown). In myocytes without an I_{TO}, the current was ~80% by 235 ms and ~50% by 1.1 s (data not shown). In either case, the noisiness and the extensive decay distinguish the outward current of the nonpregnant myocyte from that of the late-pregnant myocyte.

When elicited from −50 mV, I_{TO} was absent (Fig. 1 *B*). The slower current was about half that at HP −80 mV. This current declined to ~90% by 235 ms (Fig. 1 *C*), and to ~75% by 1.1 s. The lesser decay resembled that of the late-pregnant myocyte, but the noisiness remained.

Fig. 2, *A* and *B*, shows the typical responses of nonpregnant myocytes to a rise in $[Ca^{2+}]_o$. At HP −80 mV, when all types of K^+ channels were expressed, raising $[Ca^{2+}]_o$ to 30 mM had little effect on the average current (see small difference current in Fig. 2 *A*, A_3). At HP −50 mV, at which I_{TO} was absent, raising $[Ca^{2+}]_o$ markedly increased the total I_K (Fig. 2 *B*, B_1). The initial surge peaked at 2.8 ms and had all the kinetic features of the I_{TO} (Fig. 2 *B*, B_2). At +70 mV, the I_{TO} was 3.7× larger, and the steady state I_K (at 245 ms) was 1.9× larger than the isochronal currents in 1 mM Ca^{2+} (Fig. 2 *B*, B_3). Similar changes were seen in five other nonpregnant myocytes.

Late-Pregnant Myocytes

In late-pregnant myocytes (Fig. 1, *D–F*), the outward current first appeared at approximately −30 mV. Up to −10 mV, some outward rectification was evident, but, more positive than −10 mV, rectification was slight. The currents at all voltages have few fluctuations (smooth). Typically, they rose gradually to reach a maximum at 32.5 ± 2.1 ms (31 myocytes). Although an early rapid phase was apparent at small depolarizations from HP −80 mV (Fig. 1 *D*), no I_{TO} similar to those in nonpregnant myocytes were seen in any late-pregnant myocyte. For ~300 ms, the currents were well sustained (at ~90% by 235 ms; Fig. 1 *F*), but at >1–2 s, some decline occurred (at ~60% by 2.1 s, not shown). From HP −50 mV, the current was smaller than that from HP −80 mV, and showed similar little decay, remaining at ~90% at 235 ms, and ~80% at 2.1 s.

Fig. 2, *C* and *D*, show the typical responses of changing $[Ca^{2+}]_o$ on the I_K of two late-pregnant myocytes. Although reducing $[Ca^{2+}]_o$ to 0 mM (Fig. 2 *C*), or raising it to 30 mM (Fig. 2 *D*) led to a disappearance or an increase of the inward I_{Ca}, respectively, I_K remained virtually unchanged (see also difference currents in Fig. 2, *C*, C_3, and *D*, D_3). A similar stability of I_K in different $[Ca^{2+}]_o$ was observed in 11 other late-pregnant myocytes. In five of these, I_{Ca} had first been blocked with Co^{2+} (5 mM), and the stability of I_K was the same as those in myocytes with I_{Ca}.

Ca^{2+}-insensitive I_K as an Intrinsic Property of Late-Pregnant Uterine Myocytes

To exclude a possible artifactual nature of the unexpected Ca^{2+}-insensitive I_K of late-pregnant myocytes, we turned to evidence gathered on small multicellular preparations in which the myocytes were neither exposed to proteolytic enzymes nor their interior to EGTA. Fig. 3 shows that, in a double sucrose-gap method, such preparations produced action potentials under current-clamp conditions and ionic currents under voltage-clamp conditions. In these preparations, effects of procedures on I_K can be gauged by comparing the current at 500 ms, when the inward current had inactivated. Mn^{2+} (5 mM), which blocked the inward Ca^{2+} current, had no effect on the I_K (Fig. 3 *A*). A similar outcome was observed with Co^{2+} (3 mM; not shown). Conversely, when $[Ca^{2+}]_o$ was raised, the inward current increased, but the steady state outward current was not appreciably different (Fig. 3 *B*). These results show that Ca^{2+}-insensitive I_K is present before cell dissociation, and represents an intrinsic physiological property of late-pregnant myocytes.

Effects of Photolysis-Released $Ca^{2+}{}_i$ on I_K of Different Types of Myocytes

To avoid altering surface negative charges that can occur when manipulating $[Ca^{2+}]_o$, the effects of $[Ca^{2+}]_i$ on I_K can be tested by use of caged calcium compounds, nitr 5, and DM-nitrophene.

Nitr 5–Ca complex was diffused from the pipette solution into myocytes to which it imparted a brownish fluorescence. Unirradiated, nitr 5 had no effect on the depolarization-induced I_K, which was identical in density and kinetics to that in myocytes without nitr 5. In other control myocytes, irradiation, in the absence of

[1] *Abbreviations used in this paper:* 4-AP, 4-aminopyridine; ChTX, charybdotoxin; DTX, α-dendrotoxin; HP, holding potential; i-V, current–voltage; IbTX, iberiotoxin; I_{TO}, transient outward current; MCDP, mast-cell degranulating peptide; TEA, tetraethylammonium; V-*g*, voltage–conductance; V-*h*, voltage–steady state inactivation.

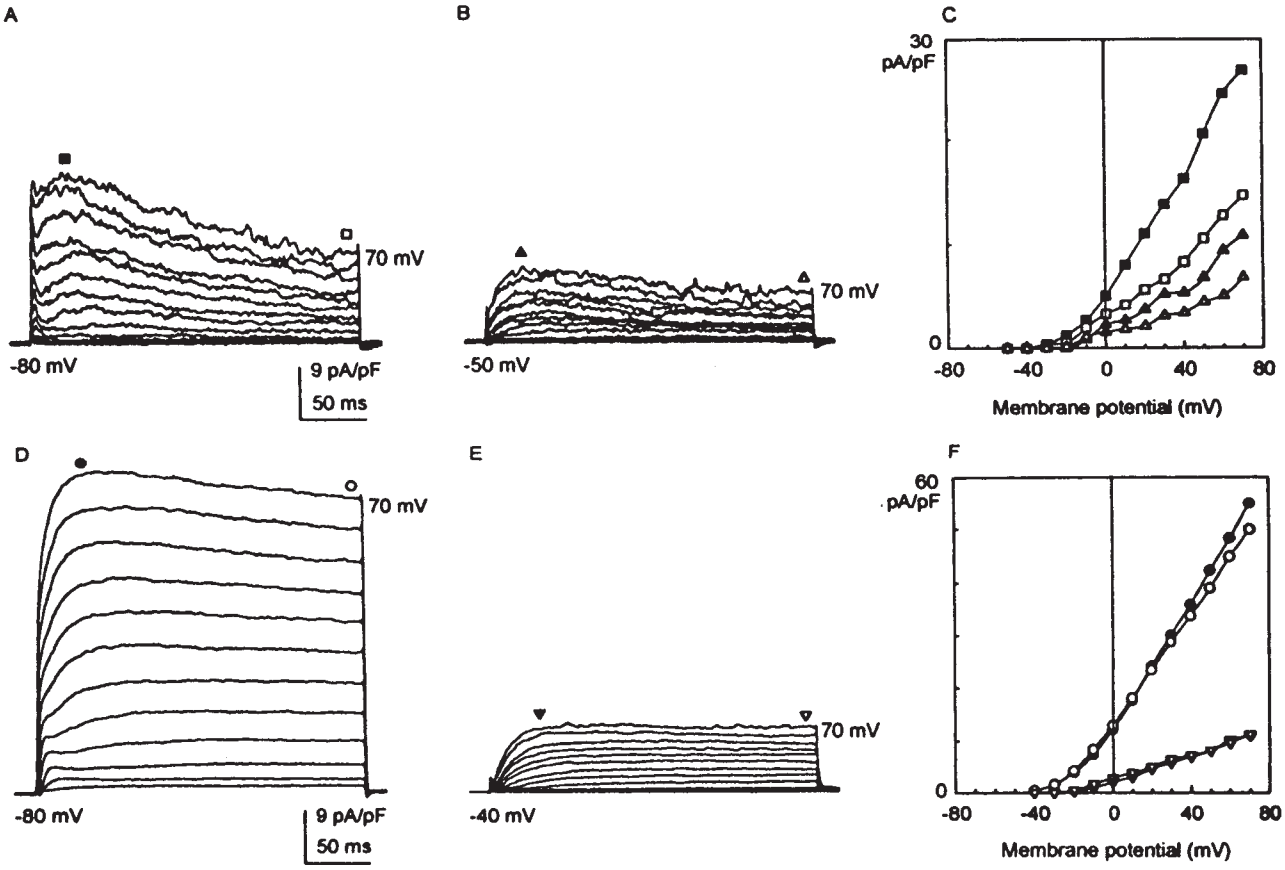

FIGURE 1. Outward currents of typical nonpregnant and late-pregnant rat uterine myocytes. Currents at HP −80 and −50 mV are shown at same scales for comparison (depolarized for 258 ms in 10-mV increments to +70 mV). Symbols above top current traces indicate where current was measured for i-V curves. (*A–C*) Nonpregnant myocytes, 16.8 pF. Current has frequent and large fluctuations (noisy). (*A*) HP −80 mV. I_{TO} is clearly visible, peaking at ~3.5 ms, declining rapidly to a more gradual current that reached maximum at 33 ms. From this maximum, decay is faster than in late-pregnant myocytes (*D*). Also note greater outward rectification. (*B*) Same myocyte, HP −50 mV. I_{TO} is now absent (see inactivation relation in Fig. 6 *A*). Maximum current is 41% of that at HP −80 mV. Current noise remains about the same; decay is less. (*C*) i-V relations. Note the differences between maximum current and end-of-pulse current, indicating degree of decay; also obvious outward rectification. (*D–F*) Myocyte from 19-d pregnant uterus; cell capacitance 108 pF. (*D*) HP −80 mV. Currents develop gradually, reaching a maximum at ~35 ms. Currents are generally smooth, with little noise fluctuations. They are also well-sustained over several hundred milliseconds. More decay is evident over several seconds. First current appeared at approximately −40 mV. Some outward rectification is evident to 0 mV; thereafter, rectification is slight. In traces from −20 to 20 mV, a small early distortion may be the transient outward current. (*E*) Same myocyte at HP −40 mV. Total current is now 17% that at HP −80 mV. No decay is evident. (*F*) i-V relations of currents at maximum and at end. Note that outward rectification is very slight, as is decay.

nitr 5, produced no effect on the depolarization-induced I_K. The effects of irradiating cells containing nitr 5–Ca complex were tested on 15 nonpregnant and 36 late-pregnant uterine myocytes, and 29 guinea pig *taenia coli* myocytes (for comparative control). Fig. 4 shows the responses in the different types of cells.

All 15 nonpregnant myocytes loaded with the nitr 5–Ca complex responded to irradiation with an increase in the I_K (Fig. 4, *A* and *B*), which averaged 4.8 ± 1.5-fold over the control (nonirradiated) I_K. The current noise was larger (Fig. 4 *B*), the holding current became slightly inward, and the tail current was bigger (Fig. 4 *A*). All these changes are consistent with an activation of a large-conductance K^+ channel.

In late-pregnant myocytes, the responses were varied. 16 myocytes (44%) showed no response (Fig. 4 *C*) and 20 myocytes (56%) showed an I_K increased by 2.0 ± 0.3-fold (Fig. 4, *D* and *E*). In all responding myocytes, the current noise increased, but an inward holding current was seen in only 13 myocytes (Fig. 4 *D*). Pooling the responding and nonresponding myocytes, the average irradiation-induced increase in I_K was 1.5 ± 0.2-fold over the control current. Thus, Ca^{2+}-activated K^+ channels, while present in late-pregnant myocytes, are expressed at a lower level.

By contrast, in guinea pig *taenia coli* myocytes in which whole-cell I_K is mostly due to large-conductance Ca^{2+}-activated K^+ channels (Yamamoto et al., 1989; Hu et al., 1989; Fan et al., 1993), 28 myocytes (97%) responded to irradiation with a 5.3 ± 0.9-fold increase in I_K (Fig. 4 *F*).

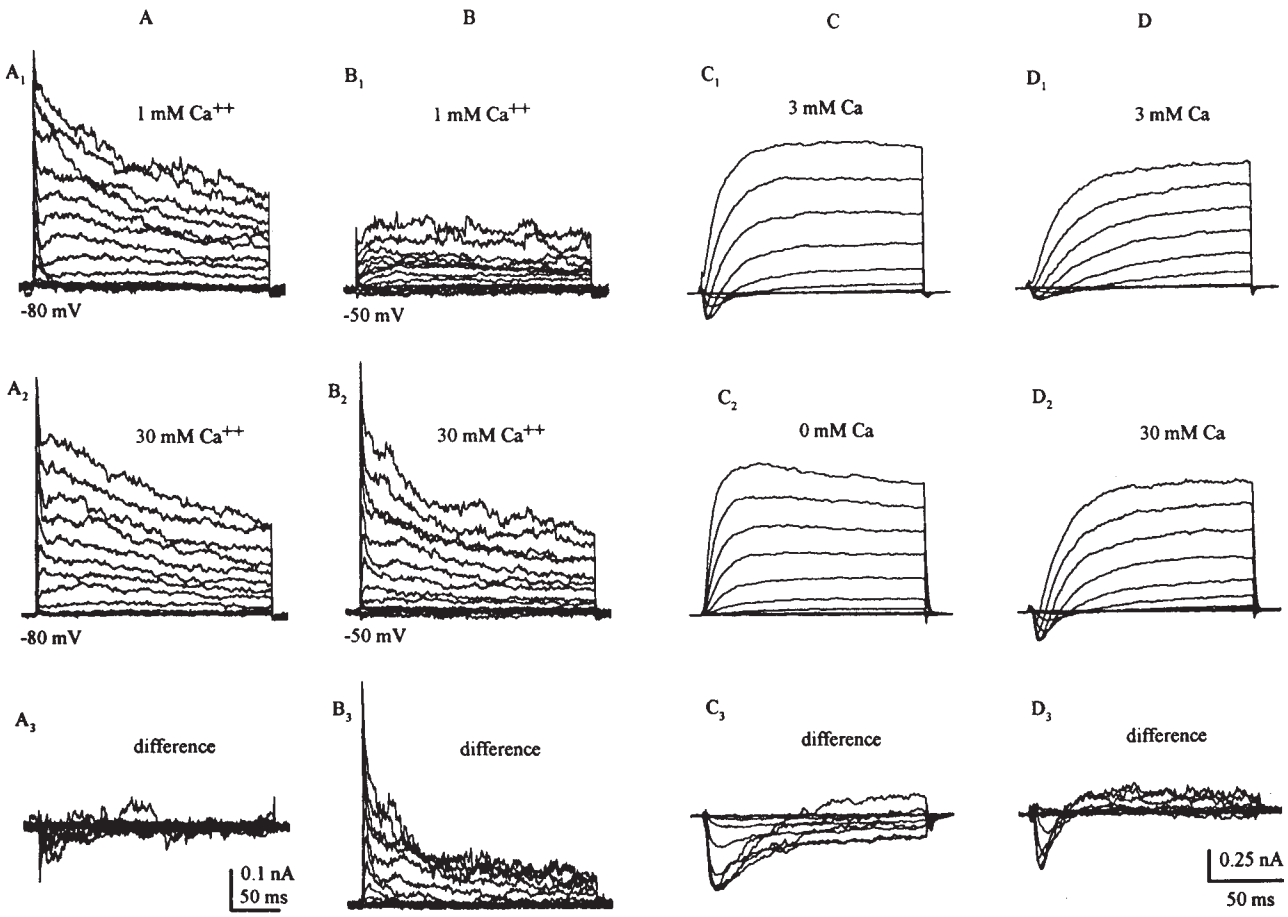

FIGURE 2. Effects of $[Ca^{2+}]_o$ on outward currents of nonpregnant and late-pregnant rat uterine myocytes. (*A* and *B*) Nonpregnant rat in estrus; cell capacitance 5.0 pF. (*A*) Holding potential −80 mV, depolarized for 245 ms in 10-mV increments to 70 mV. (A_1) In 1 mM Ca^{2+}. Note presence of a I_{TO}. (A_2) In 30 mM Ca^{2+}. Little effect, possibly because all currents are fully expressed. (A_3) Difference between currents in 30 and 1 mM Ca^{2+} verify the general lack of effects of increasing $[Ca^{2+}]_o$. (*B*) HP −50 mV; same voltage protocol. (B_1) In 1 mM Ca^{2+}, I_{TO} is inactivated; current rises gradually and is maintained for 245 ms with little decay. (B_2) 30 mM Ca^{2+}. Marked increase in outward current, mostly in I_{TO}, but also some in steady state current, as is evident in difference current (B_3). (*C* and *D*) Late-pregnant myocytes; from 17-d pregnant uterus (*C*), cell capacitance 106 pF; from 18-d pregnant uterus (*D*), cell capacitance 102 pF. Cells were held at −60 mV, and depolarized by 150-ms steps in 10-mV increments to 40 mV. (C_{1-3}) Effects of lowering $[Ca^{2+}]_o$ from 3 to 0 mM. (C_1) In 3 mM Ca^{2+}, inward I_{Ca} was present and I_K was well maintained. (C_2) In 0 mM Ca^{2+}, I_{Ca} disappeared but I_K is essentially unchanged. (C_3) Difference current between C_2 and C_1. Note that difference current represents the inward I_{Ca}, with little difference in I_K. (D_{1-3}) Effects of raising $[Ca^{2+}]_o$ from 3 to 30 mM. Conventions similar to those in C_{1-3}. (D_1) In 3 mM Ca^{2+}, I_{Ca} and I_K serve as bases for comparison. (D_2) In 30 mM Ca^{2+}, I_{Ca} increased appreciably, but I_K remained essentially unchanged. (D_3) Difference current shows changes in I_{Ca}, but little change in I_K.

To address possible species differences, in three myocytes from the analogous rat cecum, irradiation increased the average I_K by 21.9 ± 3.3-fold above the control level.

DM-nitrophene (Kaplan, 1990) was tested on 24 late-pregnant myocytes. The qualitative changes observed with DM-nitrophene were similar in every respect to those seen using nitr 5-Ca: the irradiation-induced increases in $[Ca^{2+}]_i$ always caused much smaller increases in I_K in late-pregnant uterine myocytes than in *taenia coli* myocytes.

PARADIGM FOR ANALYZING WHOLE-CELL I_K OF UTERINE MYOCYTES

From the evidence presented above, the whole-cell I_K of nonpregnant and late-pregnant uterine myocytes are complex and substantially different from each other. In the following, we will attempt to sort and apportion the components of I_K in each type of myocyte.

Basis of Paradigm: Steady State Availability of K^+ Currents

Fig. 5 shows the voltage–steady state inactivation (V-*h*) relation of the outward current, obtained on eight nonpregnant and seven late-pregnant myocytes. Each myocyte was held at −80 mV, first subjected to a 10-s conditioning voltage step, and then to a 180-ms test step of up to +70 mV to elicit outward currents. The data are complex, and can only be fitted by assuming the presence of three populations of currents with distinct Boltzmann

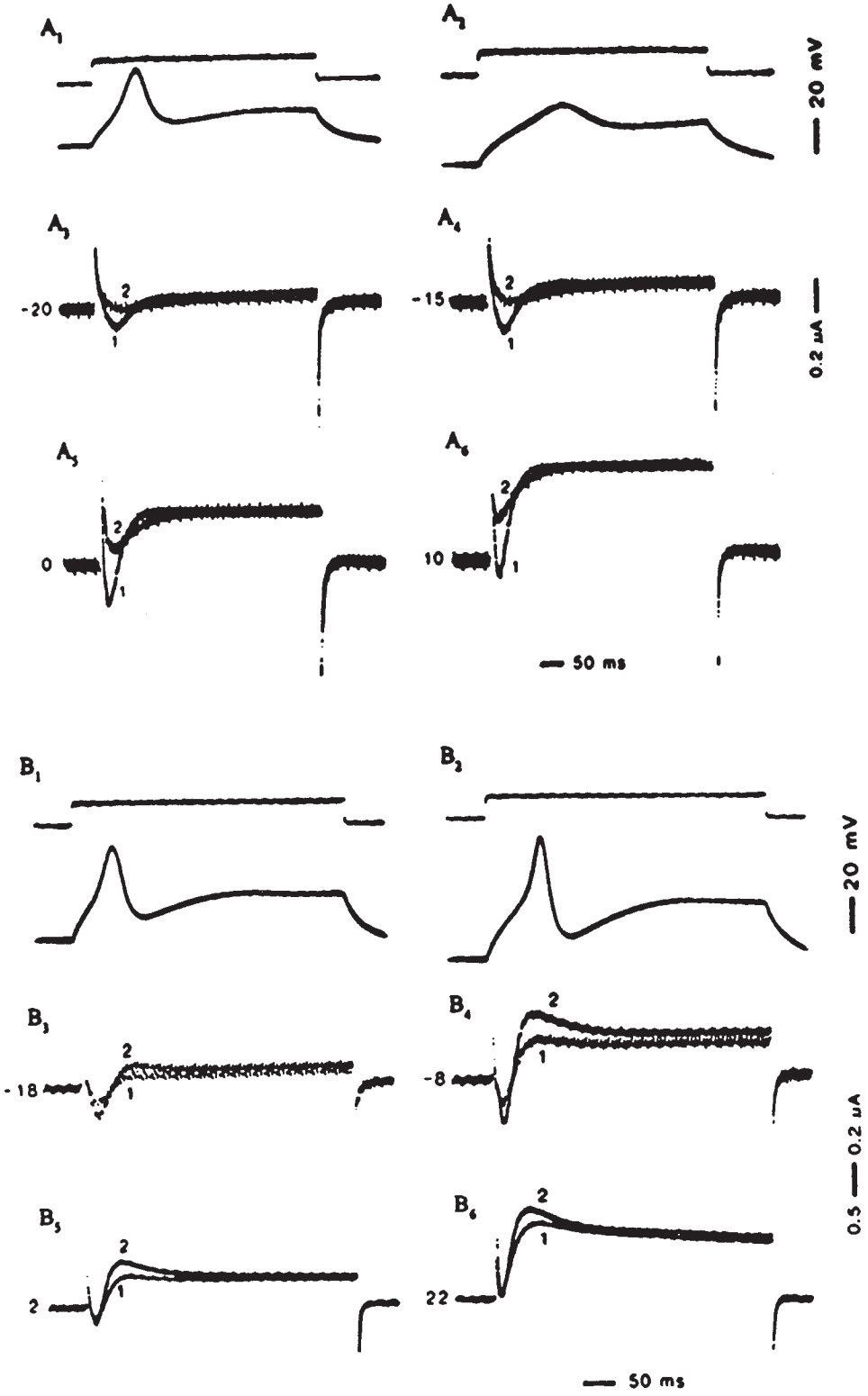

FIGURE 3. Responses of small multicellular preparations of late-pregnant myometrium to conditions that affect inward I_{Ca}. Double sucrose-gap method. (*A*) Effects of Mn^{2+} (5 mM). Preparation from 19-d pregnant uterus. Total "nodal" capacitance, 0.1 μF. (A_1) Action potential elicited by constant current step. (A_2) Action potential after 5 min of superfusion with Krebs solution containing Mn^{2+}, showing blockade. (A_{3-6}) Superimposed composite currents under voltage-clamp conditions. Numbers at left margin of each trace represent command voltage step. Traces marked 1 are from control conditions, traces marked 2 are from after treatment with Mn^{2+}. Note that whereas Mn^{2+} effectively blocked inward I_{Ca}, it produced no detectable changes in steady state I_K. (*B*) Effects of increasing $[Ca^{2+}]_o$ from 1.9 to 8 mM. Preparation from 20-d pregnant uterus. Total nodal capacitance, 0.07 μF. (B_1) Action potential elicited by constant current in 1.9 mM Ca^{2+}. (B_2) Action potential in 8 mM Ca^{2+} shows a faster rate of rise and a higher amplitude, consistent with increased I_{Ca}. (B_{3-6}) Superimposed composite currents under voltage-clamp conditions. Traces marked 1 are from 1.9 mM Ca^{2+}, traces marked 2 are from 8 mM Ca^{2+}. Because of limitations of method, effects of procedures on I_K can only be examined at steady state (500 ms) when inward current has inactivated. Note that, whereas increased $[Ca^{2+}]_o$ increased I_{Ca} and increased overlap artifact in the early part of the outward current, it did not produce significant changes of steady state I_K. The constancy of I_K in these preparations, which were not treated with enzymes and their myocyte interior was not exposed to EGTA, is consistent with similar observations made on dissociated myocytes.

distribution functions. Two of the components inactivate at depolarized potentials, whereas a third does not. For nonpregnant myocytes (Fig. 5 *A*), the inactivating components represent 59 (C_1) and 30% (C_2) of the total current, with half-inactivating voltages at −59.5 and −22.9 mV, respectively. The noninactivating component (C_3) represents 11% of the current. For late-pregnant myocytes (Fig. 5 *B*), the inactivating components are 67% for C_1 and 23% for C_2, with half-inactivation voltages, respectively, at −62.7 and −21.2 mV. The noninac-

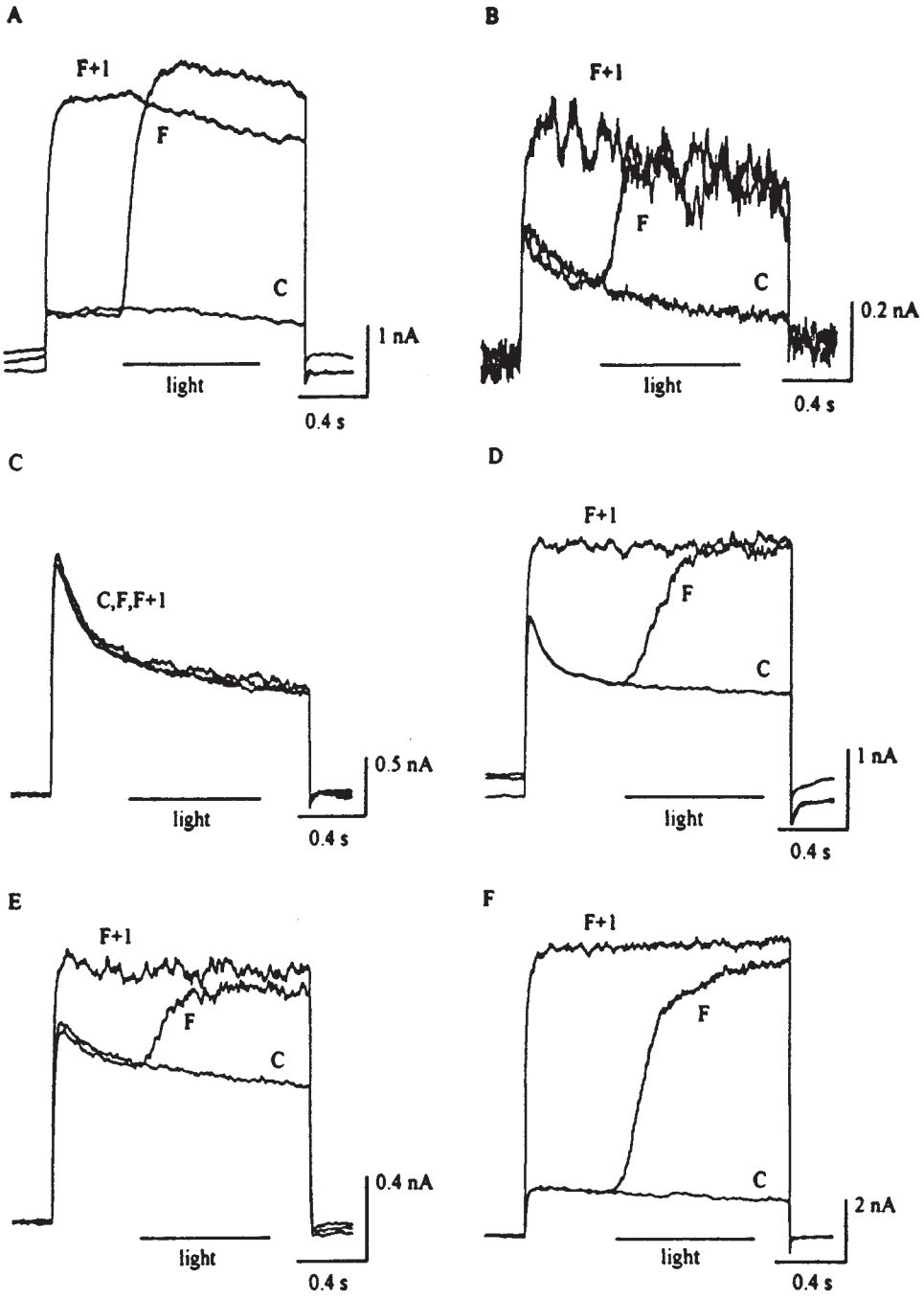

FIGURE 4. Effects of photolysis-induced increase of $[Ca^{2+}]_i$ on nonpregnant, late-pregnant uterine myocytes and on *taenia coli* myocyte. Caged nitr 5–Ca complex was introduced intracellularly by diffusion from pipette (see text for details). In each panel, five consecutive traces, recurring at 3-s intervals, are shown. Traces marked C represent three superimposed traces of depolarization-induced whole-cell I_K in cells that have been loaded with nitr 5–Ca complex, but not irradiated. Traces marked F represent the fourth trace, during which myocyte was exposed to 360 nm light at time indicated by bar beneath traces. Traces marked F+1 represent the fifth trace in series. (*A* and *B*) Nonpregnant myocytes, 10.6 and 8.4 pF, respectively. In *A*, average I_K showed an increase upon irradiation. The increase in this cell is unusually large. Other changes also evident include more prominent current noise, downward shift of baseline, indicating holding current became more inward, and larger tail current. In *B*, increase in current noise is especially evident. (*C–E*) Late-pregnant myocytes; from 18-d pregnant uterus, 78 (*C*) and 60 (*D*) pF, and 19-d pregnant uterus, 120 pF (*E*). These examples show representative responses in late-pregnant myocytes. (*C*) Typical of 44% of test samples (36 myocytes), this cell showed no response. (*D*) In this myocyte, in addition to an increase in average I_K, there was an inward shift of holding current, an increase in tail current, and an increase of current noise. (*E*) In this myocyte, response consisted of an increase in average I_K and in current noise. 56% of all samples responded as in *D* and *E*. (*F*) Response of a representative *taenia coli* myocyte, which is known to have abundant maxi-K channels. Large increase in average I_K and increase in current noise occurred in 97% of 29 cells tested.

tivating component (C_3) represents 10% of the total. Thus, in pregnancy, the C_1 component enlarged at the expense of the C_2 component.

These results suggest that a paradigm using holding potentials, −80, −40 (or −50), and 0 mV, can sort the whole-cell I_K into smaller components. Holding at 0 mV gives the noninactivating component (C_3). Holding at −40 mV gives the C_2 and C_3 components, whereas the difference between these currents yields the C_2 component. Holding at −80 mV gives the total I_K, and the difference between currents from HP −80 and −40 mV yields the C_1 component. Thus, currents in the C_3 component are excluded from the C_2 component, as are currents in the C_2 and C_3 components from the C_1

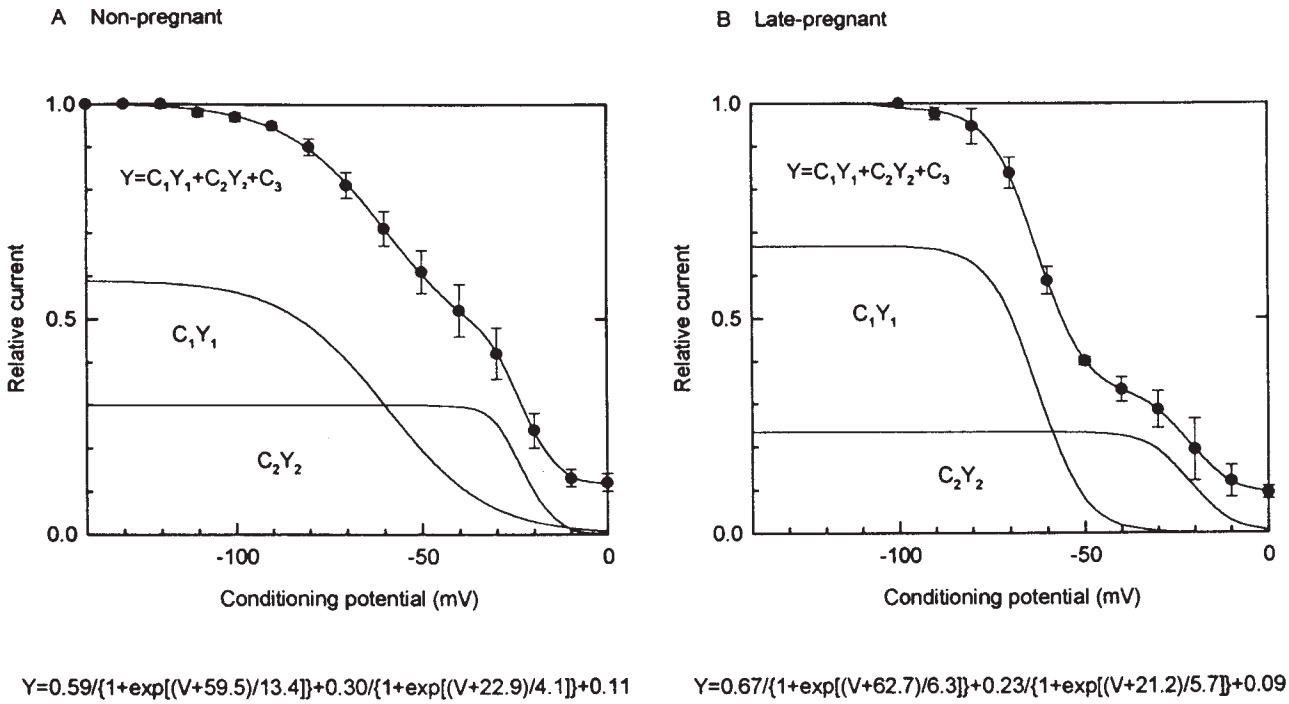

FIGURE 5. Voltage–steady state inactivation relation of outward current in nonpregnant and late-pregnant myocytes. Two-step protocol, holding potential −80 mV, conditioning step 10 s duration, test step 180 ms. Current of test step in presence and absence of the conditioning step is plotted on ordinate as relative current. Conditioning voltage on abscissa. Symbols are data (means ± SEM). (*A*) Nonpregnant myocytes. Data from eight myocytes (9.2, 18, 9.2, 11, 15.4, 25, 13.6, and 16.4 pF). The complex relation requires three components for fitting. C_1, comprising 59% of total K^+ current, is half inactivated at −59.5 mV, with a slope factor of 13.4 mV. C_2, comprising 30%, is half inactivated at −22.9 mV with a slope of 4.1 mV. C_3, comprising 11%, does not inactivate. (*B*) Late-pregnant myocytes. Data from seven myocytes; three from 17-d pregnant uteri (89, 58, and 82.4 pF); two from 18-d pregnant uteri (80 and 96 pF), and two from 19-d pregnant uteri (93 and 180.4 pF). The complex relation also requires three components: C_1, comprising 67% of total I_K, is half inactivated at −62.7 mV, with a slope factor of 6.3 mV; C_2, comprising 23%, is half inactivated at −21.2 mV, with a slope factor of 5.7 mV; and C_3, comprising 10%, does not inactivate. Although the half-inactivation voltages and slope factors are similar to those of nonpregnant myocytes, C_1 has enlarged at the expense of C_2.

component. A residue of C_1 currents remains in the combined C_2, C_3 components, but its relative size can be estimated from the V-*h* curves.

This paradigm can be assessed by evaluating the average current densities (Table I) observed on a larger sample of myocytes used in other experiments. From a group of nonpregnant myocytes, separate from those used in the V-*h* study, the total current density at HP −80 mV was 41.4 pA/pF (Table I). On the basis of the V-*h* relation (Fig. 5 *A*), this total might be apportioned as: C_1, 24.4 pA/pF (59%); C_2, 12.4 pA/pF (30%), and C_3, 4.6 pA/pF (11%). Outward currents elicited from HP −40 mV contain components C_2 and C_3, which are the same as above, and a residue of C_1, which is 10.7% (Fig. 5 *A*) or 4.4 pA/pF. So, the deduced total current for HP −40 mV is 21.4 pA/pF, which can be compared with the observed value of 21.6 pA/pF (Table I).

For late-pregnant myocytes, the total outward current elicited from HP −80 mV was 40.1 pA/pF (Table I), which can be apportioned as: C_1, 26.9 pA/pF (67%); C_2, 9.2 pA/pF (23%), and C_3, 4 pA/pF (10%). At HP −50 mV, the C_2 and C_3 components are the same as above, and the residual C_1 (8.3%; Fig. 5 *B*) is 3.3 pA/pF. Therefore, the total deduced current for HP −50 mV is 16.5 pA/pF, which is close to the observed current of 17.1 pA/pF (Table I).

The paradigm was further tested by gauging the sizes of the various components on six late-pregnant myocytes. Each of these cells was held successively at −80, −40, and 0 mV, and I_K at +70 mV and 200 ms were compared. The fractional sizes were: C_1, 0.67 ± 0.07 (six myocytes); C_2, 0.23 ± 0.04; and C_3, 0.09 ± 0.03, comparable with those derived from the V-*h* relations (Fig. 5 *B*).

Such close agreements support a general usefulness of the paradigm. Although each component still contains multiple currents, there are fewer and some overlap can be estimated. For clarity of later presentation, we will refer to the various components by their pregnancy status and designation as used in Fig. 5. Thus, I_{LP1} refers to the C_1 component of late-pregnant myocytes, and I_{NP2} refers to the C_2 component of nonpregnant myocytes, etc. When two components are not separated, they are designated as the sum of the two, $I_{LP2,3}$, etc.

TABLE I

Some Properties of I_K of Uterine Myocytes

	Total current				
	Nonpregnant			Late-pregnant	
HP (mV)	−80*	−80	−40	−80	−50
t_{max} (ms)	3.8 ± 0.5	24.8 ± 2.6		32.5 ± 2.1	
	(10)	(12)		(31)	
I_{max} (pA/pF)	68.0 ± 11.3	41.4 ± 7.5	21.6 ± 3.2	40.1 ± 1.7	17.1 ± 1.3
	(10)	(12)	(12)	(31)	(31)

	Components of I_K					
	I_{NP1}	I_{NP2}	I_{NP3}	I_{LP1}	I_{LP2}	I_{LP3}
g (μS/cm²)	493 ± 68	118 ± 27	15 ± 3	254 ± 20	64 ± 14	33 ± 9
	(7)	(7)	(7)	(22)	(11)	(12)
$V_{0.5,act}$ (mV)	7.2	3.9	39.1	7.7	4.2	63.4
	(7)	(7)	(7)	(22)	(11)	(12)
$V_{0.5,inact}$ (mV)	−59.5	−22.9	—	−62.7	−21.2	—
	(8)	(8)		(7)	(7)	

All values are means ± SEM, with number of myocytes used in parentheses. t_{max}, time to reach maximum value; I_{max}, maximum current; *transient outward current. g, maximum conductance taken at 120 mV. $V_{0.5}$ values are for half activation or half inactivation.

COMPONENTS OF THE WHOLE-CELL K^+ CURRENT

Because the components contain fewer overlapping currents than the whole-cell I_K, detailed scrutiny of their kinetic and steady state activation and inactivation properties (see Fig. 6), their Ca^{2+} sensitivity (see Fig. 7), and their susceptibility to blocking agents (see Figs. 8–12) may lead to a better understanding of the differences between nonpregnant and late-pregnant uterine myocytes.

Component Currents of Nonpregnant Myocytes

Transient outward current. I_{TO} was isolated as the difference current between currents elicited from holding potentials −80 and −50 mV. In 11 of 21 nonpregnant myocytes examined, a distinct I_{TO} was seen. In late-pregnant myocytes, a small transient surge was sometimes seen at small depolarizations, but positive to −10 mV, no current of similarly fast kinetics was ever prominent. Therefore, I_{TO} is discussed here as a K^+ current exclusively of nonpregnant myocytes.

I_{TO} activated with an exponential time course; the time-constant (τ) was slightly voltage dependent, averaging 3 ms at −10 mV and 1.5 ms at +60 and +70 mV. However, the variations were large, possibly because of variations in the ambient temperature during the experiment (see Conner and Stevens, 1971). I_{TO} inactivated with a τ of 3 ms that was not voltage dependent.

The voltage–conductance (V-g) relations of I_{TO} followed Boltzmann distribution closely, with half-activation at 5 mV and a slope of 24.3 mV (Fig. 6 *A*). The maximum conductance was 664 ± 106 μs/cm² (nine myocytes). The voltage–inactivation relation obtained in a two-step command protocol showed half-inactivation at −76.5 mV, with a slope of 6.9 mV (Fig. 6 *A*). By −40 mV, only 0.1% of I_{TO} was available.

Other K^+ currents. The other K^+ currents of nonpregnant myocytes are analyzed by using myocytes that had no I_{TO}. The development and decay of I_{NP1} (difference current between those from HP −80 and −40 mV) and I_{NP2} (difference current between HP −40 and 0 mV) were exponential. The activation was voltage dependent, and τ for I_{NP1} (10 ± 2 ms at +20 mV, 6 ± 1 ms at +70 mV; 11 myocytes) was faster than τ for I_{NP2} (19 ± 3 ms at +20 mV, 9 ± 2 ms at +70 mV; 4 myocytes). The activation of I_{NP3} (HP 0 mV) was instantaneous. The inactivation of I_{NP1} was voltage independent, with an average τ of 110 ms. I_{NP2} and I_{NP3} did not decay over 1.2 s.

In Fig. 6, the steady state activation and inactivation properties of I_{NP1} (Fig. 6 *B*), I_{NP2} (Fig. 6 *C*), and I_{NP3} (Fig. 6 *D*) are shown in hollow symbols, and their Boltzmann distributions in full lines. Half-activation voltages and the associated slopes are given in Table I, as are the maximum conductances. The V-h relations in Fig. 6, *B* and *C*, were rescaled from Fig. 5 *A*, and the half-inactivation voltages and associated slopes are given in Table I. In both cases, there was an overlap with the activation curves, encompassing 12% of the maximum at −40 mV for I_{NP1}, and 30% of the maximum at −20 mV for I_{NP2}.

When $[Ca^{2+}]_o$ was increased from 1 to 30 mM, the activation curves of both I_{NP1} and $I_{NP2,3}$ shifted to the positive, with the $V_{0.5,\ act}$ moving 14 and 16 mV, respectively (Fig. 7, *A* and *B*).

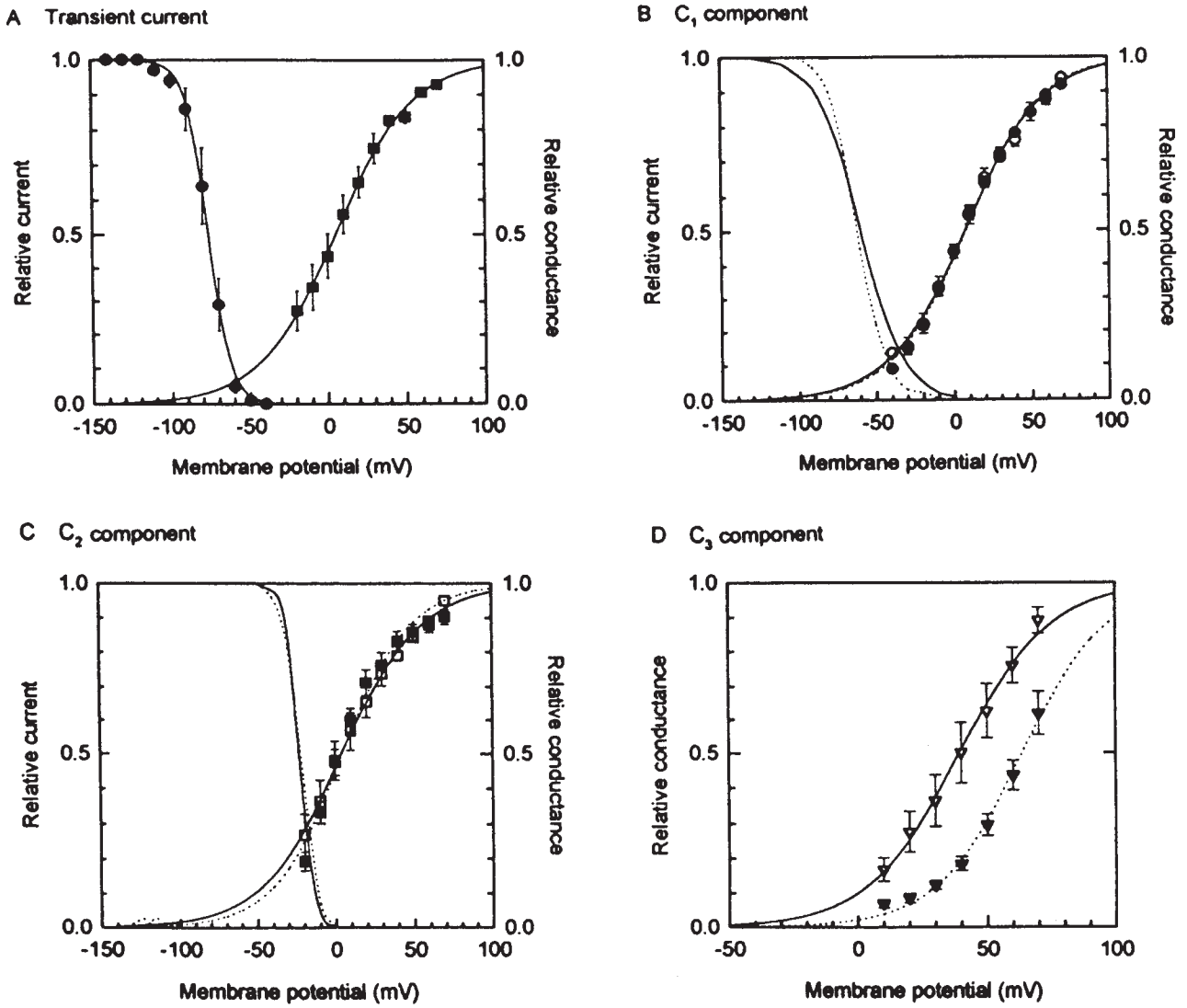

FIGURE 6. Steady state activation and inactivation properties of component currents of nonpregnant and late-pregnant uterine myocytes. (*A*) Properties of I_{TO} in nonpregnant myocytes. For V-*h* relation (*left curve* and *ordinate*; data from six myocytes shown as means ± SEM, if scatter is larger than symbol), two-pulse protocol similar to those for Fig. 5 was used. Solid curve is Boltzmann distribution function with half inactivation at −76.5 mV and a slope of 6.9 mV. At −50 mV, the relative current is 0.01; at −40 mV, 0.001. For V-*g* relation (*right curve* and *ordinate*; eight myocytes), relative conductance as a function of maximum conductance was obtained for each myocyte as the asymptotic value at 120 mV. Half activation is at +5 mV with a slope factor of 24.3 mV. (*B–D*) Properties of component currents. See test for paradigm of extracting C_1, C_2, and C_3 currents. In these panels, data from nonpregnant myocytes are represented by hollow symbols and their Boltzmann distribution by solid lines. Data from late-pregnant myocytes are represented by filled symbols, and their Boltzmann distribution functions by broken lines. In *B* and *C*, V-*h* relations are rescaled from Fig. 5. (*B*) Properties of C_1 currents. For nonpregnant myocytes (data from seven myocytes which had no I_{TO}), half activation is at 7.2 mV with a slope factor of 24.6 mV. For late-pregnant myocytes (data from 22 myocytes), half activation is at 7.7 mV with a slope factor of 23.7 mV. "Window current" is present in both types of myocytes. (*C*) Properties of C_2 currents. For nonpregnant state (seven myocytes), half activation is at 3.9 mV with a slope factor of 17.7 mV. For late-pregnant state (11 myocytes), half activation is at 4.2 mV with a slope of 22.1 mV. Window currents are larger than those in C_1 currents. (*D*) Properties of C_3 currents that do not inactivate. For nonpregnant state (seven myocytes), half activation is at 39.1 mV, slope 17.7 mV. For late-pregnant state (12 myocytes), half activation is at 63.4 mV, slope 16.7 mV. Half-activation voltages are significantly different (see text for details).

Component Currents of Late-Pregnant Myocytes

The development and decay of I_{LP1} and I_{LP2} were also exponential. Activation of both currents were voltage dependent; τ for I_{LP1} was faster (10 ± 1 ms at +20 mV; 4 ± 0.4 ms at +70 ms; 20 myocytes) than τ for I_{LP2} (18 ± 1 ms at +20 ms; 9 ± 1 ms at 70 mV; 20 myocytes), but neither rate was significantly different from the corresponding rate of nonpregnant myocytes. The activation of I_{LP3} was instantaneous. The decay of I_{LP1} could be described by two exponential terms; the faster term was

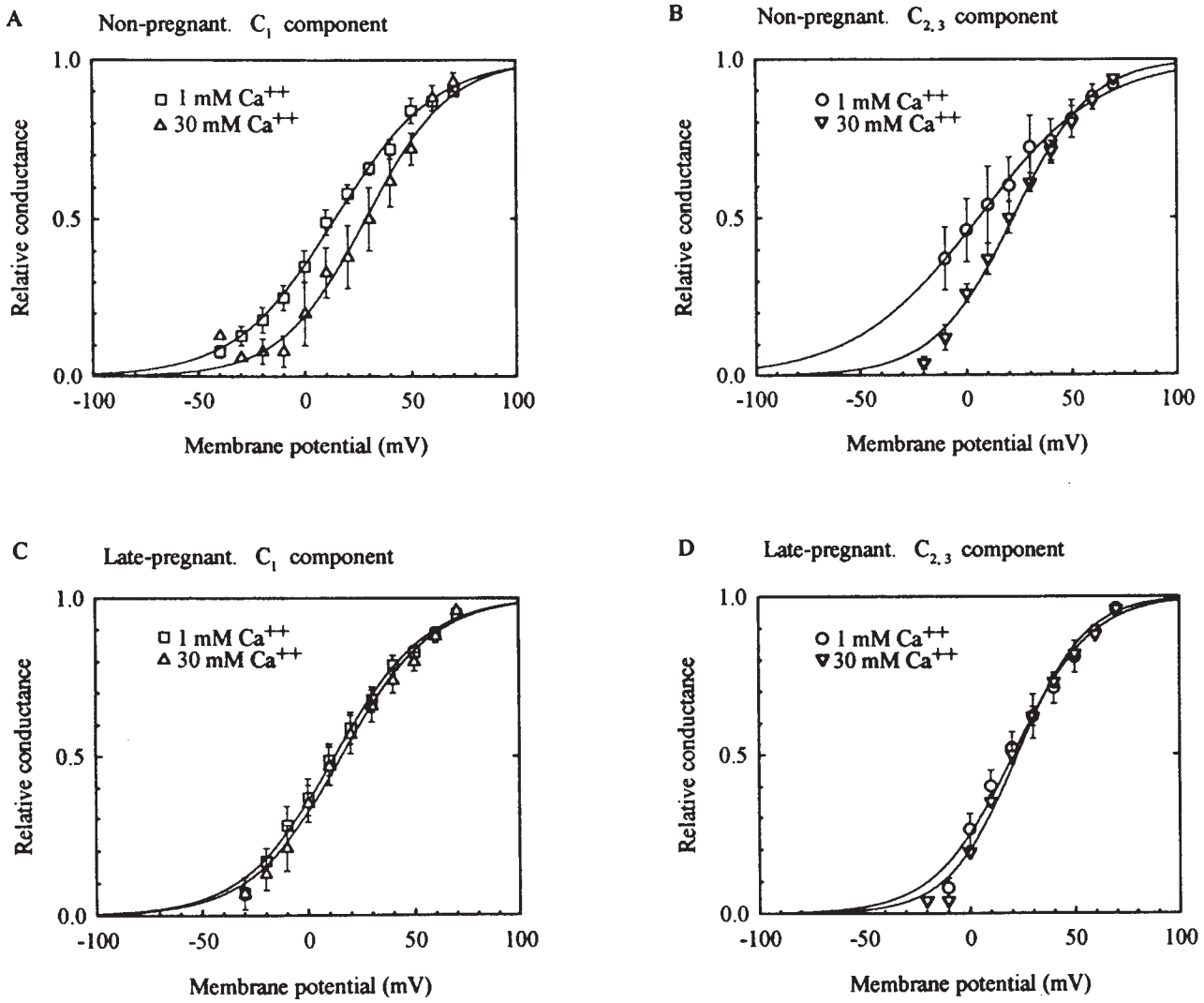

FIGURE 7. Effects of $[Ca^{2+}]_o$ on activation of component currents of whole-cell I_K in nonpregnant and late-pregnant uterine myocytes. Symbols represent means ± SEM of five nonpregnant (*A* and *B*) and nine late-pregnant myocytes (*C* and *D*). Solid lines represent Boltzmann distributions. In nonpregnant but not late-pregnant myocytes, 30 mM Ca^{2+} caused a positive shift of V-*g* relation.

voltage dependent and stabilized at ~200 ms, whereas the slower term was voltage independent at ~2.5 s. I_{LP2} and I_{LP3} showed little decay over 2.1 s.

The steady state activation and inactivation properties of I_{LP1}, (Fig. 6 *B*), I_{LP2} (Fig. 6 *C*), and I_{LP3} (Fig. 6 *D*) are shown in Fig. 6 as filled symbols, and their Boltzmann distributions in broken lines, for comparison with those of nonpregnant myocytes. Their half-activation voltages and the associated slopes as well as their maximum conductances are given in Table I. The V-*h* relations in Fig. 6, *B* and *C*, were rescaled from Fig. 5 *B*, and the half-inactivation voltages and associated slopes are given in Table I. Regions of overlap with the activation curves are similar to those seen in nonpregnant myocytes.

Unlike nonpregnant myocytes, increasing $[Ca^{2+}]_o$ to 30 mM caused no significant shifts in the activation curve of any of the component currents of late-pregnant myocytes (Fig. 7, *C* and *D*).

Among many similarities in the component currents of nonpregnant and late-pregnant myocytes, significant

TABLE II

Percent of Whole-Cell I_K Susceptible to Blocking Agent

	Myocyte	
Blocking agent	Nonpregnant	Late-pregnant
TEA, 0.5 mM	35	19
Charybdotoxin, 100 nM	21	13
Iberiotoxin, 1 nM	30	18
Apamin, 100 nM	0	5
4-aminopyridine, 5 mM	56	50
α-dendrotoxin, 200 nM	0	19
Mast cell degranulating peptide, 100 nM	0	4

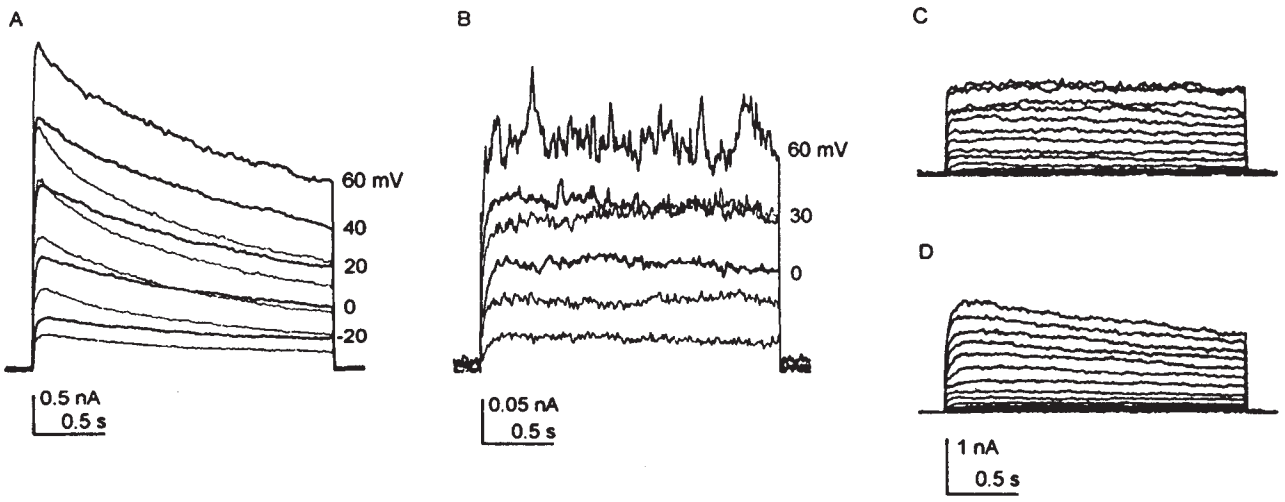

FIGURE 8. Effects of tetraethylammonium chloride on component currents of I_K of late-pregnant uterine myocytes. (*A–C*) TEA, 0.5 mM. (*D*) TEA, 2 mM. In *A* and *B*, traces of residual current in TEA (I_{TEA}, *light traces*) are overlaid on traces of current before TEA ($I_{control}$, *heavy traces*) at same voltages. For clarity, only selected traces are shown. (*A*) Myocyte from 20-d pregnant uterus, 191 pF. Traces shown are I_{LP1}'s, which are difference currents between those obtained at HP −90 and −40 mV. (*B*) Traces shown are $I_{LP2,3}$, obtained directly by recording at HP −40 mV. TEA reduction of average current is associated with marked reduction of peak-to-peak current fluctuations. The *y*-axis labels (*0, 30,* and *60 mV*) identify $I_{control}$ current records of $I_{LP2,3}$(*heavy traces*), and 0.5 mM TEA causes reductions in the current at each voltage step (*light traces, below*). At faster time scales (not shown), TEA does not affect activation kinetics (for 60-mV step, $\tau_{control}$ = 13 ms, τ_{TEA} = 15 ms). (*C*) Difference currents, $I_{control} - I_{TEA}$ at all voltage steps for myocytes in *A*, representing currents blocked by TEA (5.7 pA/pF at 60 mV), which does not decay over 2.1 s. Calibrations are the same as in *A*. (*D*) TEA, 2 mM. Myocyte from 17-d pregnant uterus; 126.6 pF. Traces are difference currents, $I_{control} - I_{TEA}$, at all voltages. Although it caused a greater block (12.6 pA/pF at 60 mV, 2.1 s) than other higher concentrations, their effects involve also some decaying component, making them less useful for differentiating channel types.

differences were found in three areas: maximum conductances of their C_1 components (493 μS/cm² for I_{NP1} vs. 254 μS/cm² for I_{LP1}; $P < 0.001$ by *t* test); the steady state half-activation voltages of their C_3 components (39.1 mV for I_{NP3} vs. 63.4 mV for I_{LP3}; $P = 0.004$); and their responses to raised Ca^{2+} concentrations in the bath. These differences underlie important characteristics of the whole-cell K^+ currents (see DISCUSSION).

PHARMACOLOGICAL RESPONSES OF MYOMETRIAL K^+ CHANNELS

As the total I_K is separated into smaller units by different holding potentials, additional use of selective blocking agents may identify some individual channel types and reveal their contributions to the total current (Table II).

Tetraethylammonium Ion

Fig. 8 shows the typical actions of tetraethylammonium (TEA) on I_{LP1} and $I_{LP2,3}$ of late-pregnant myocytes. At 0.5 mM, TEA appreciably reduced the average current (Fig. 8, *A* and *B*) as well as the current noise at all voltages (Fig. 8 *B*). Similar effects were seen in nonpregnant myocytes. The noisiness of the affected component and its stability over 2.1 s (see difference currents, $I_{control} - I_{TEA}$, Fig. 8 *C*) suggest that only a large-conductance channel was blocked. In 2 mM or higher concentrations, the blocked current also contained an early decaying phase (Fig. 8 *D*), possibly attributable to additional channel types. Therefore, for differentiating channel types, we will focus on the effects of 0.5 mM TEA.

On average, the TEA-sensitive component in I_{LP1} amounted to 17% ($I_{TEA}/I_{control}$ = 0.83 ± 0.09, five myocytes), which contributed 11% of the total I_K (0.17 × 0.67; see Fig. 5 *B*). On $I_{LP2,3}$, the TEA-sensitive component represented 26% ($I_{TEA}/I_{control}$ = 0.74 ± 0.11, five myocytes). As it contained a residue of 8.3% of I_{LP1}, the blocked fraction in the $C_{2,3}$ components was 24%, which contributed 8% (0.24 × 0.33) of the total I_K. Thus, the susceptible current(s) represented 19% of the total I_K of late-pregnant myocytes (Table II).

In nonpregnant myocytes, the blocked fraction in I_{NP1} was 36%, which contributed 21% (0.36 × 0.59) of the total I_K. In $I_{NP2,3}$, the blocked fraction after correction for residual I_{NP1} was 33%, contributing 14% (0.33 × 0.41) of the total current. In sum, the TEA-sensitive component constituted 35% of the total I_K of nonpregnant myocytes (Table II).

Charybdotoxin

This peptidyl toxin from the scorpion, *Leiurus quinquestriatus*, blocks several Ca^{2+}-activated K^+ channels and also voltage-gated potassium channels (Miller et al., 1985; Garcia et al., 1995). It was tested on three nonpregnant and seven late-pregnant myocytes at 100 nM (IC_{50}, 100 pM, Vasquez et al., 1989). On nonpregnant

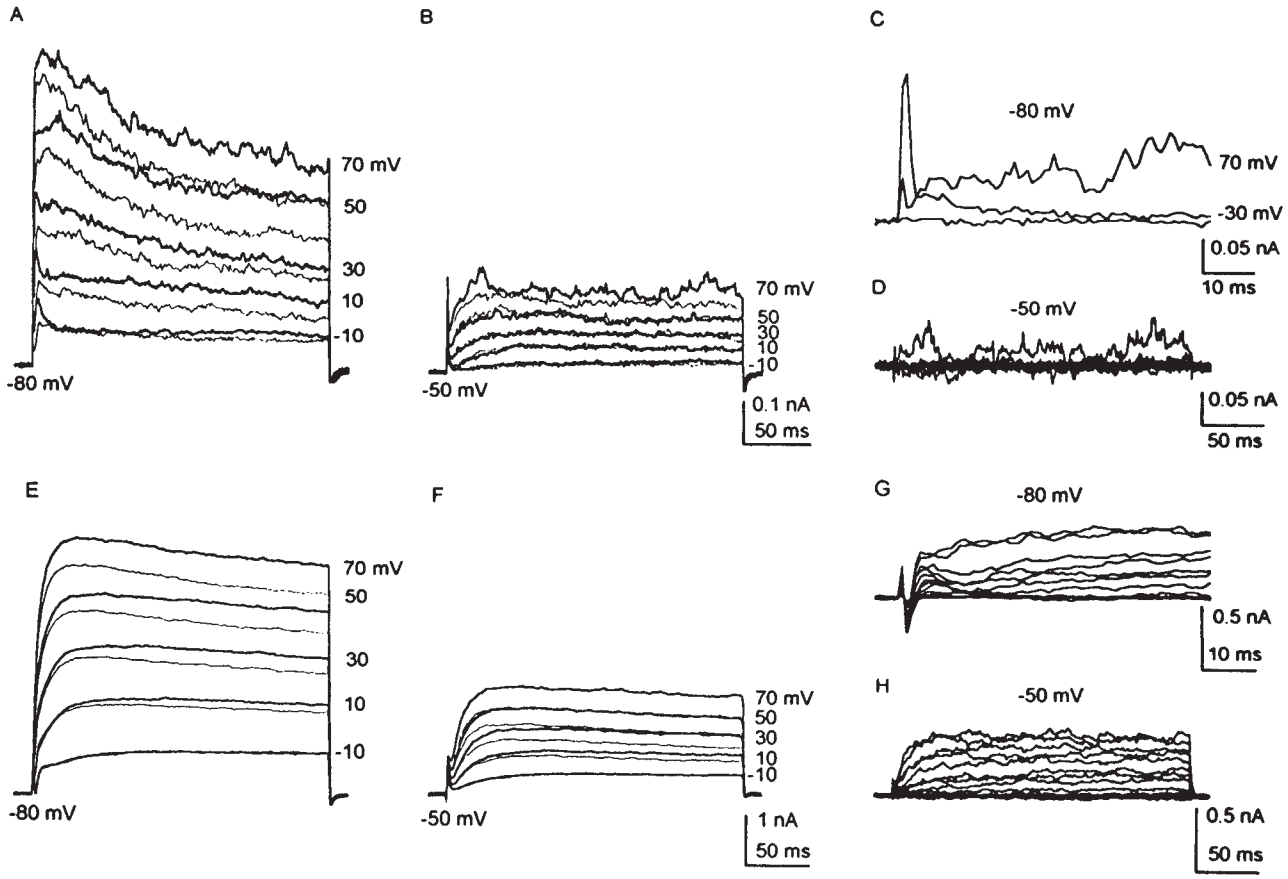

FIGURE 9. Effects of charybdotoxin (100 nM) on I_K of uterine myocytes. Conventions are similar to those in Fig. 8, except that *A* and *E* represent directly recorded total currents; I_{ChTX} (*light traces*) overlaid on $I_{control}$ (*heavy traces*). (*C, D, G,* and *H*) are different currents, or currents blocked by ChTX. (*A–D*) Nonpregnant myocyte. 18.4 pF. ChTX reduced peak-to-peak current fluctuations. In *A*, I_{TO} is distinct in traces of −10, 10, and 30 mV in $I_{control}$, and is blocked by ChTX. In *B*, at HP −50 mV, only $I_{NP2,3}$ is elicited. Effects of ChTX are rather small, and are not manifested until more positive than 50 mV. (*C*) Difference currents, $I_{control} - I_{ChTX}$ at HP −80 mV. For clarity, only two traces at fast time scale are shown. Note the particularly prominent block on the I_{TO}, manifested here as an initial surge, peaking at 3 ms. The subsequent current seen in the 70-mV trace is clearly of a different and noisy type. In the full trace (not shown), the blocked current shows no decay. (*D*) Difference currents, $I_{control} - I_{ChTX}$ at HP −50 mV confirm that ChTX had no effect until beyond 50 mV. (*E–H*) Myocyte from 20-d pregnant uterus; 117.6 pF. At HP −80 (*E*) and −50 (*F*) mV, I_{ChTX} for the −10-mV trace is superimposed on $I_{control}$. (*G*) Difference currents, $I_{control} - I_{ChTX}$ for HP −80 mV, on a fast time scale. The blocked currents show an initial hump, contrast with the blocked I_{TO} in *C*, followed by another sustained current. (*H*) Difference currents, $I_{control} - I_{ChTX}$ at HP −50 mV.

myocytes, charybdotoxin (ChTX) reduced the I_{TO} (Fig. 9 *A*), the average current, and the current noise. The susceptible current(s) (as $I_{control} - I_{ChTX}$, Fig. 9, *C* and *D*) had three components: an I_{TO} that peaked at ~3 ms and was already present at −30 mV; a noisy current in I_{NP1} (at 30 and 50 mV, Fig. 9 *A*) that was inactivated at HP −50 mV (for eliciting $I_{NP2,3}$, Fig. 9 *B*); and another that appeared at voltages positive to 50 mV (Fig. 9 *D*). The blocked fraction in I_{NP1} represented 24%, contributing 14% of the total current. In $I_{NP2,3}$, the blocked fraction less the residual I_{NP1} was 18%, contributing 7% of the total. In sum, ChTX blocked 21% of the whole-cell I_K of nonpregnant myocytes (Table II).

On late-pregnant myocytes (Fig. 9, *E–H*), the main effect of ChTX was a reduction of the average current (Fig. 9, *E* and *F*). Although outward currents were already evident at −30 to 0 mV, the susceptible current(s) did not appear till 10 mV, and increased with more positive voltages (Fig. 9 *E*). The blocked current had two components: an early part that peaked at ~10 ms, and a late part that had a noisiness and activation similar to those in nonpregnant myocytes (Fig. 9 *G*). In $I_{LP2,3}$ (Fig. 9 *F*), the susceptible current rose gradually over ~25 ms, and did not decay over 230 ms (Fig. 9 *H*), but it differed from its counterpart in nonpregnant myocytes in emerging at a much less positive voltage of 10 mV. In I_{LP1}, the blocked fraction averaged 9%, contributing 6% of the total I_K. In $I_{LP2,3}$, the blocked fraction after correction for residual I_{LP1} averaged 21%, contributing 7% of the total current. In sum, 13% of the whole-cell I_K of late-pregnant myocytes were susceptible to ChTX (Table II).

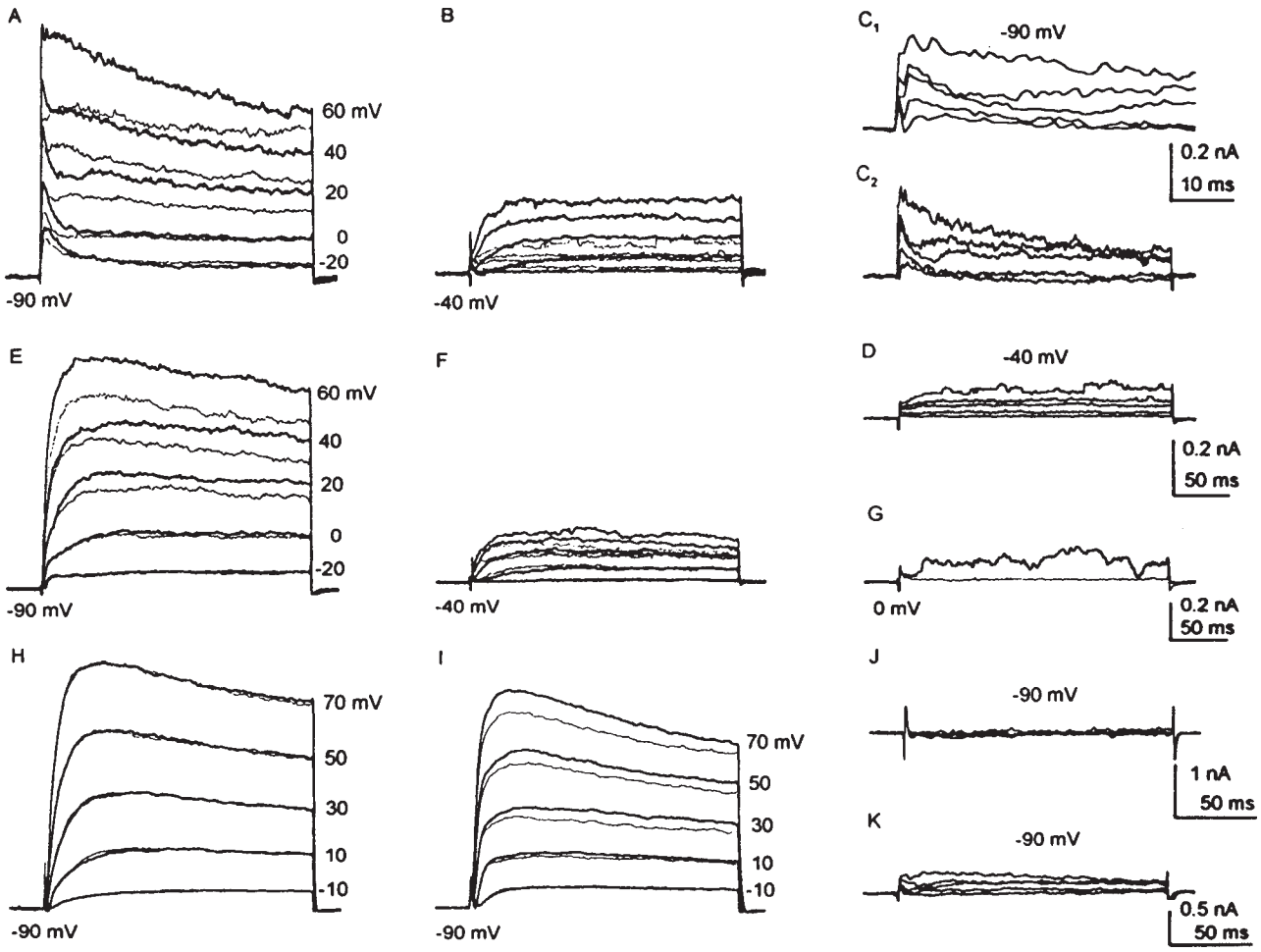

FIGURE 10. Effects of iberiotoxin (1 nM) on I_K of uterine myocytes. Selected traces for clarity. I_{IbTX} traces are lighter and overlaid on $I_{control}$ traces from the same voltages. (*A–D*) Nonpregnant myocyte with I_{TO}; 18 pF. (*A*) HP −80 mV, showing total I_K. (*B*) HP −40 mV, showing $I_{NP2,3}$ for same voltage steps as in *A*. (*C*) Difference currents, $I_{control} - I_{IbTX}$ at HP −80 mV, (*C_1*) at a fast time scale to show that initial part of the blocked current coincided with I_{TO}. (*D*) Difference currents at HP −40 mV. (*E–G*) Nonpregnant myocyte without I_{TO}; 18 pF. (*E*) HP −80 mV. (*F*) HP −40 mV. Traces are of same voltages as in *E*. (*G*) HP 0 mV, showing I_{NP3}. IbTX reduces peak-to-peak fluctuations and average currents, most notably in I_{NP3}, but also evident in directly recorded currents (*A, B, E,* and *F*), and as difference currents (*C* and *D*). Other features of note: (*a*) IbTX effect is not evident until V > 20 mV (*A* and *E*), probably because susceptible current is not activated; (*b*) IbTX blocks a part of the I_{TO} at all voltages (*A* and *C_1*), but the blocked current is different from that blocked by ChTX (Fig. 9), suggesting that I_{TO} is not a homogenous current; (*c*) unlike most maxi-K currents shown, some IbTX-susceptible currents show an appreciable rate of decay (*C_2*). (*H–K*) Late-pregnant myocytes. (*H*) Myocyte from an 18-d pregnant uterus, 105.4 pF. HP −90 mV. This myocyte has very little IbTX-susceptible currents, as can also be seen in difference currents in *J*. (*I*) Myocyte from 18-d pregnant uterus, 137 pF. Main responses are similar to those described for nonpregnant myocyte. Difference currents are shown in *K*.

Iberiotoxin

This peptidyl toxin from the scorpion, *Buthus tamulus*, is more potent ($IC_{50} \approx 25$ pM) and more specific than ChTX for the large-conductance Ca^{2+}-activated K^+ channel (Galvez et al., 1990). It was tested at 1 nM concentration on four nonpregnant and four late-pregnant myocytes. Fig. 10 shows the typical effects on two nonpregnant myocytes (Fig. 10, *A–G*) and two late-pregnant myocytes (Fig. 10, *H–K*). The effects were qualitatively similar: it reduced the average current and the current noise (Fig. 10 *G*). The predominant susceptible current was nondecaying, but sometimes an early decaying component was seen (Fig. 10 *C*). The effects on I_{TO} differed from those of ChTX: the I_{TO} at small depolarizations were minimally affected, but I_{TO} at more positive voltages were blocked, indicating that myometrial I_{TO} originated from more than a single channel type. On I_{NP1}, the blocked fraction averaged 17% (four myocytes), contributing 10% of the total I_K. On $I_{NP2,3}$, the blocked fraction after correction for residual I_{NP1} averaged 48%, contributing 20% of the total I_K. In sum, 30% of the whole-cell I_K of nonpregnant myocytes were susceptible to iberiotoxin (IbTX; Table II).

On some late-pregnant myocytes, IbTX had no effect (Fig. 10 *H*). On average, the blocked fraction of I_{LP1} av-

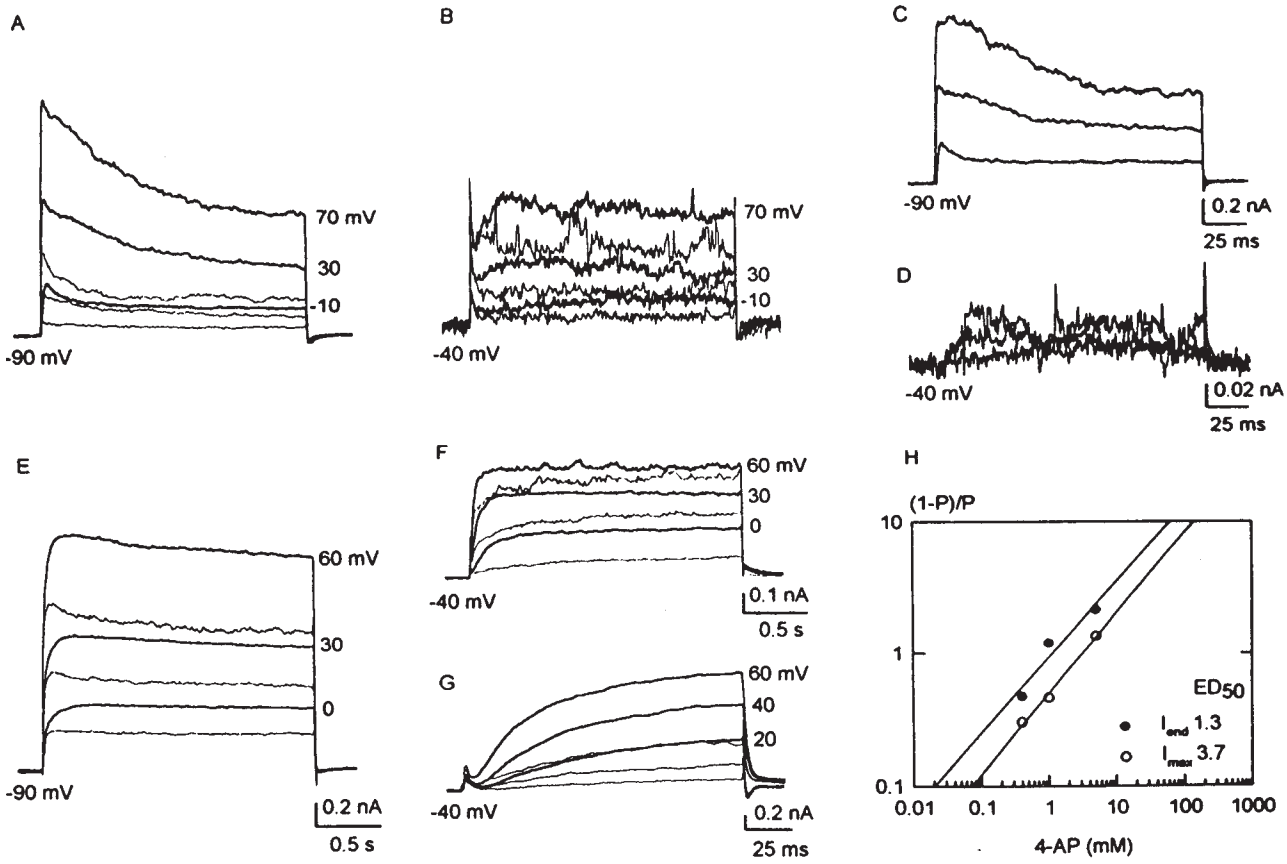

FIGURE 11. Effects of 4-aminopyridine on I_K of uterine myocytes. Selected traces for clarity. $I_{4\text{-}AP}$ (*light traces*) overlaid on $I_{control}$ of same voltage steps. (*A–D*) Nonpregnant myocyte with I_{TO}, 15.6 pF. 4-AP, 5 mM. While 4-AP markedly reduced total I_K (*A*) and $I_{NP2,3}$ (*B*), it did not block the I_{TO} (*A*), as also shown in difference currents in *C*. It also did not reduce current fluctuations in direct recording (*B*), or in difference currents (*D*). These effects are consistent with 4-AP actions on K_v channels. (*E–G*) Myocyte from 18-d pregnant uterus. 162 pF. 4-AP, 1 mM. (*E*) HP −90 mV, showing total I_K. Note that current at 2.1 s (end of step) is slightly more depressed by 4-AP than current at 35 ms (maximum), a feature also seen in dose–response relations in *H*. (*F* and *G*) HP −40 mV, showing $I_{LP2,3}$. Noisy current is obvious at +60 mV, but 4-AP has no effect on peak-to-peak fluctuations. Slowing of the rate of activation by 4-AP is already evident, but more so at a faster time scale in *G*. At 60 mV, $\tau_{control}$ = 36 ms, $\tau_{4\text{-}AP}$ = 64 ms. This effect on kinetics could cause the wrong conclusion that 4-AP is selective for some transient current. Comparing *E* and *F*, and also *A* and *B*, it is clear that main effects of 4-AP are exerted on the C_1 components (I_{LP1} and I_{NP1}). (*H*) Dose–response relation of 4-AP on currents at 35 ms (I_{max}; *hollow symbols*) and at 2.1 s (*filled symbols*). Hill plot, abscissa, log concentration; ordinate, (1 − P)/P where P is $I_{4\text{-}AP}/I_{cont}$. ED_{50} is at 1 − P/P = 1. I_K at 2.1 s is almost three times more susceptible than I_{max}.

eraged 8%, comprising 5% of the total current. On $I_{LP2,3}$, the blocked fraction after correction for residual I_{LP1} averaged 39%, contributing 13% of the total current. In sum, 18% of the whole-cell I_K of late-pregnant myocytes were susceptible to IbTX (Table II).

Apamin

This toxin from the venom of honey bees blocks a small-conductance K^+ channel that is sensitive to Ca^{2+}, but not to voltage (Romey et al., 1984; Blatz and Magleby, 1986). It (100 nM) was tested on one nonpregnant and five late-pregnant myocytes. On the former, it had no detectable effects. On the latter, it had no effect on I_{LP1} ($I_{apamin}/I_{control}$ = 1.00 ± 0.02, five myocytes), but blocked 15% of $I_{LP2,3}$ ($I_{apamin}/I_{control}$ = 0.85 ± 0.02), which should affect 5% of the total I_K.

4-Aminopyridine

Three concentrations of 4-aminopyridine (4-AP), 0.4, 1, and 5 mM, were tested on two nonpregnant and six late-pregnant myocytes (Fig. 11). Their actions were similar in both types of myocytes, and they differed from those of TEA, ChTX, or IbTX: (*a*) the noisy current fluctuations were unaffected (Fig. 11, *B* and *F*); (*b*) it slowed the activation of $I_{LP2,3}$ (Fig. 11, *F* and *G*), resulting in a seemingly greater effect at 150 ms ($I_{4\text{-}AP}/I_{control}$ = 0.38 ± 0.03, six myocytes) than at 2.1 s ($I_{4AP}/I_{control}$ = 0.78 ± 0.03); and (*c*) it hastened the decay of the TEA-insensitive component in I_{LP1}. These effects occurred with all three concentrations, being most marked in 5 mM. On I_{LP3}, 5 mM 4-AP had no effect. In I_{LP1}, the blocked fraction averaged 48%, comprising 32% of the total I_K. After correction for residual I_{LP1},

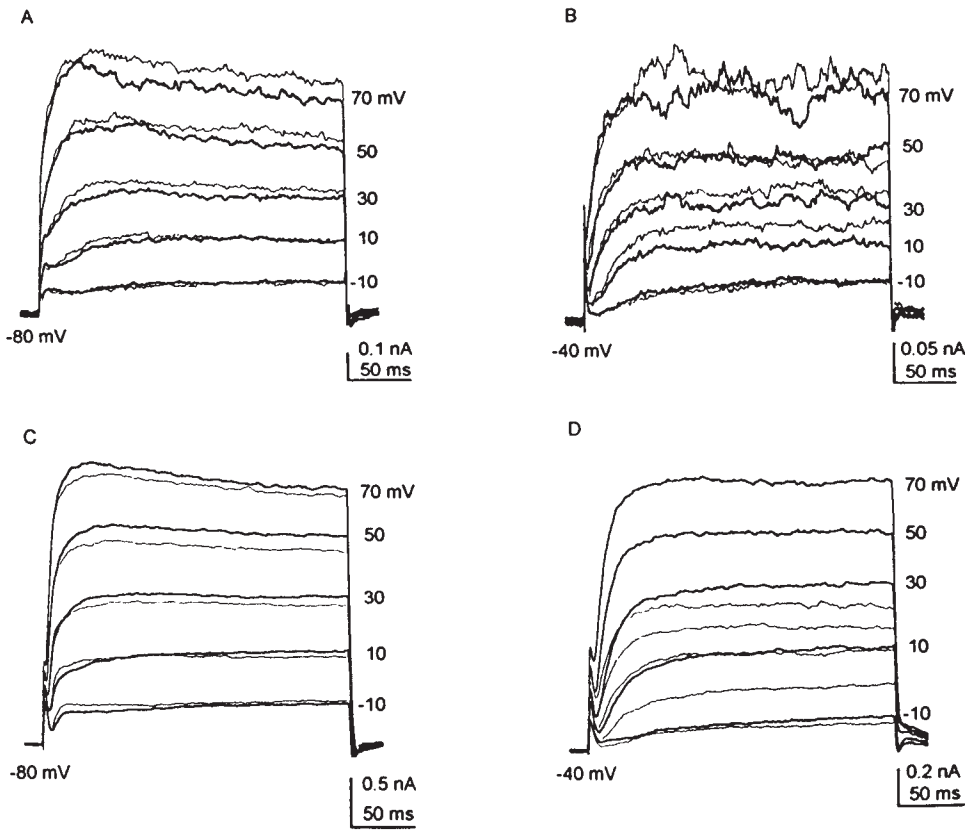

FIGURE 12. Effects of dendrotoxin (200 nM) on I_K of uterine myocytes. In all panels, I_{DTX} (*light trace*) is overlaid on $I_{control}$. For clarity, only selected traces are shown. (*A* and *B*) Nonpregnant myocyte, 19.2 pF. (*A*) HP −80 mV, eliciting total I_K. (*B*) HP −40 mV, eliciting $I_{NP2,3}$. DTX has no effect on this myocyte. (*C* and *D*) Myocyte from 19-d pregnant uterus, 93.2 pF. (*C*) HP −80 mV. Total I_K is reduced slightly by DTX (I_{DTX}/I_{cont} = 0.96 at maximum current and 0.97 at end). (*D*) HP −40 mV. DTX effect on $I_{LP2,3}$ is appreciable (I_{DTX}/I_{cont} = 0.54 at maximum and at end). Note that in DTX, current fluctuations are unchanged. Effects are consistent with DTX blocking a delayed rectifier current (see text for details).

the blocked fraction in $I_{LP2,3}$ averaged 56%, comprising 18% of the total current. In sum, 50% of the whole-cell I_K of late-pregnant myocytes were susceptible to 4-AP (Table II).

Significantly, in nonpregnant myocytes, the I_{TO}, peaking at ~3 ms, was not preferentially blocked (Fig. 11 *A*; also dose–response relations in Fig. 11 *H*). The blocked fraction of I_{NP1} averaged 73%, comprising 43% of the total outward current. After correction for residual I_{NP1}, the blocked fraction of $I_{NP2,3}$ averaged 32%, comprising 13% of the total current. In sum, 56% of the whole-cell I_K of nonpregnant myocytes were susceptible to blockade by 4-AP (Table II).

α-Dendrotoxin

This member of a group of peptidyl toxins from the venom of mamba snakes (*Dendroaspis augusticeps*) blocks a gradually activating and slowly decaying voltage-gated channel of small conductance that shows little outward rectification (see Dreyer, 1990). It was tested on five nonpregnant and four late-pregnant myocytes at 200 and 400 nM. On the former, α-dendrotoxin (DTX) had no effect (Fig. 12, *A* and *B*). On late-pregnant myocytes, DTX did not reduce current fluctuations and was more effective in blocking $I_{LP2,3}$ (I_{DTX}/I_{cont} = 0.60 ± 0.10, four myocytes) than I_{LP1} (I_{DTX}/I_{cont} = 0.90 ± 0.10; Fig. 12, *C* and *D*). Thus, the fractions blocked were 37% (after correction for residual I_{LP1}) and 10%, respectively, contributing 12 and 7% of the total I_K, for a sum of 19% (Table II; observed $I_{DTX}/I_{control}$ for whole-cell I_K = 0.82 ± 0.02; four myocytes).

Mast-Cell Degranulating Peptide

Mast-cell degranulating peptide (MCDP), a peptidyl toxin from honey bee venom, blocks the same class of delayed rectifier as DTX (Stansfeld et al., 1987; Brau et al., 1990; Dreyer, 1990). It was applied to four late-pregnant myocytes at 100 nM. There was little effect on I_{LP1}. Its effects were confined to the $I_{LP2,3}$, reducing the average current ($I_{MCDP}/I_{control}$ = 0.89 ± 0.03) without affecting current fluctuations. The deduced effect on the whole-cell I_K is 3.6% (Table II; observed I_{MCDP}/I_{cont} = 0.96 ± 0.02; four myocytes).

Table II summarizes the effects of the various agents. Allowing for some overlapping actions, a combination of ChTX, IbTX, and 4AP on nonpregnant myocytes, and additionally of apamin and DTX on late-pregnant myocytes, blocked all outward currents. The data show (*a*) K_{Ca} currents constitute a smaller fraction of the total outward current in late-pregnant than in nonpregnant myocytes, and (*b*) DTX-susceptible K_v currents are present in late-pregnant but not in nonpregnant myocytes.

SINGLE-CHANNEL OBSERVATIONS

To resolve an apparent contradiction between the presence of K_{Ca} channels in late-pregnant uterine myocytes

and the Ca^{2+} insensitivity of their whole-cell I_K, we conducted some single-channel studies on detached inside-out patches of the surface membrane, focussing on the large-conductance Ca^{2+}-activated K^+ (maxi-K) channel. As reference, we used patches from *taenia coli* myocytes that contained abundant maxi-K channels (Hu et al., 1989; Fan et al., 1993).

In patches from *taenia coli* myocytes, openings of single K^+ channels, often in multiples, were seen in every patch, yielding an average of 2.7 channels per patch. In these, the 150-pS channel openings predominated (>95%). In patches from late-pregnant uterine myocytes, single channel activities were rarer; 8 of 51 (15.7%) randomly made patches showed no openings of any type, and in many patches only one channel was present, yielding an average of 1.8 channels per patch. In them, single-channel activities were also more complex. Of 92 single channels, the frequency of occurrence of various types (by their unitary conductance and charge-carrier) were: 140-pS K^+ channels, 60.8%; 50-pS K^+ channels, 7.6%; 20-pS K^+ channels, 16.3%; 400-pS Cl^- channels, 15.2%. However, when by chance a patch contained both small- and large-conductance channels, the small-conductance channels were usually much more active than the large-conductance channels, as evident in Fig. 13, *A* and *B*.

The myometrial maxi-K channels exhibited readily detectable activities at approximately −30 mV, and the current–voltage (i-V) relation in asymmetric K^+ distribution (K_i/K_o = 5.4/135) showed significant outward rectification. They had a unitary conductance of 139 ± 3 pS (at 0 mV; n = 24), and, by extrapolation of the −30 to 0 mV segment of the i-V curve, a zero-current voltage at −83 mV (expected Nernst potential, −82 mV).

Influence of Voltage and $[Ca^{2+}]_i$ on P_o of Maxi-K^+ Channels

Comparing *taenia* and myometrial patches, there are differences in the open probability of the maxi-K channels, voltage–P_o relations, and the sensitivity of P_o to internal Ca^{2+} concentrations. Fig. 14, *A* and *B*, shows the V-P_o relations of two representative channels, one from a *taenia* myocyte and the other from a uterine myocyte, at pCa's 7 and 8. Fig. 14 *C* summarizes such data from six *taenia* channels and nine myometrial channels. Several features are readily apparent. (*a*) The slopes of the curves (*k*), representing that the logarithmic voltage dependence of P_o is shallower for the myometrial channel (10.5 ± 0.9 mV at pCa 8; 12.2 ± 1.6 mV at pCa 7) than for the *taenia* channel (7.6 ± 0.6 mV at pCa 8; 8.6 ± 0.7 mV at pCa 7). By *t* test, the difference in pCa 8 is significant (P = 0.05), whereas the difference in pCa 7 is not (P = 0.12). (*b*) The voltage at which P_o = 0.5 (V_h; i.e., when a channel is equally likely to be open as closed) is more positive for the myometrial channel (86.8 ± 9.1 mV at pCa 8; 68.3 ± 9.1 mV at pCa 7) than for the *taenia* channel (49.7 ± 5.4 mV at pCa 8; 24.1 ± 5.2 mV at pCa 7). The difference for either pCa is significant (P = 0.004 for pCa 8, and 0.012 for pCa 7). (*c*) The negative shift of V_h when pCa is changed from 8 to 7 is less in the myometrial channel (18 mV) than in the *taenia* channel (26 mV).

From Fig. 14 *C*, it is readily apparent that within the physiological range of voltages (−40 to +30 mV), the open probability at a fixed pCa in the myometrial maxi-K channel is only ~0.05–0.1 that of the *taenia* channel.

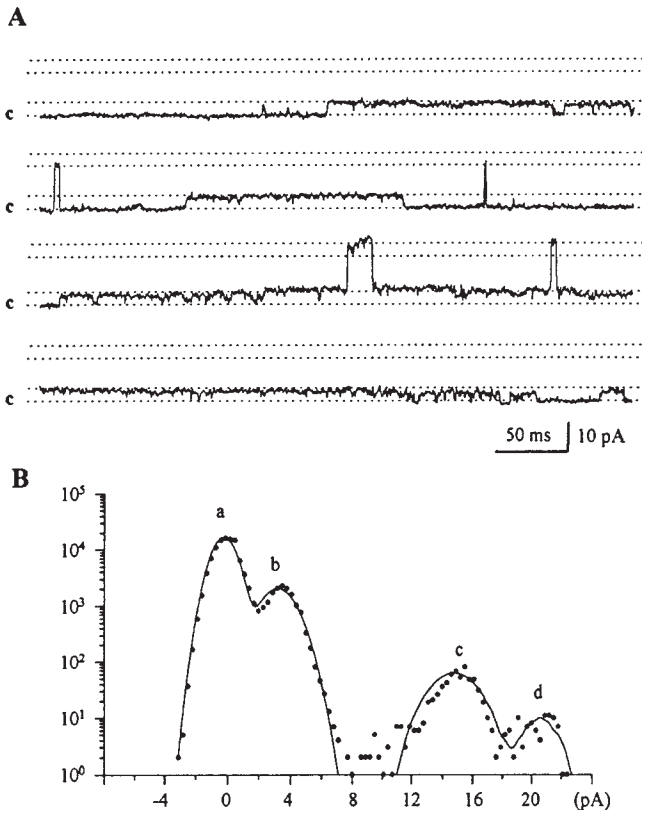

FIGURE 13. Relative activities of small and large-conductance K^+ channels in membrane patch from late-pregnant uterine myocyte. (*A*) Detached inside-out patch from 18-d pregnant uterine myocyte. Holding potential +40 mV. Pipette solution (facing outside of membrane, mM): 135 NaCl, 5.4 KCl, 1 $CaCl_2$, 1 $MgCl_2$, 10 HEPES, 5 glucose. Bath solution (facing inside of membrane, mM): 135 KCl, 0.6 EGTA, 0.1 $CaCl_2$ (pCa = 8), 10 HEPES. This patch has both small- and large-conductance channels, infrequently encountered in uterine myocyte patches. Closed state (*c*) marked at left margin. Dotted lines indicate different open levels: first level is for small-conductance channel, second level is for large-conductance channel, third level is for simultaneous openings of small and large channels. Unit conductance for small channel is 41 pS; for large channel, 180 pS. (*B*) Activity histogram of channels in *A*. Abscissa in 0.1 pA bins; ordinate in log scale, total data points, each representing 150-μs duration (in a 16-s continuous recording). Peak *a* represents closed state, *b* a small-conductance channel alone, *c* a large-conductance channel alone, and *d* a small and large channel simultaneously. P_o for the large channel is 0.007 and for the small channel is 0.15 (21× higher; see text for other details).

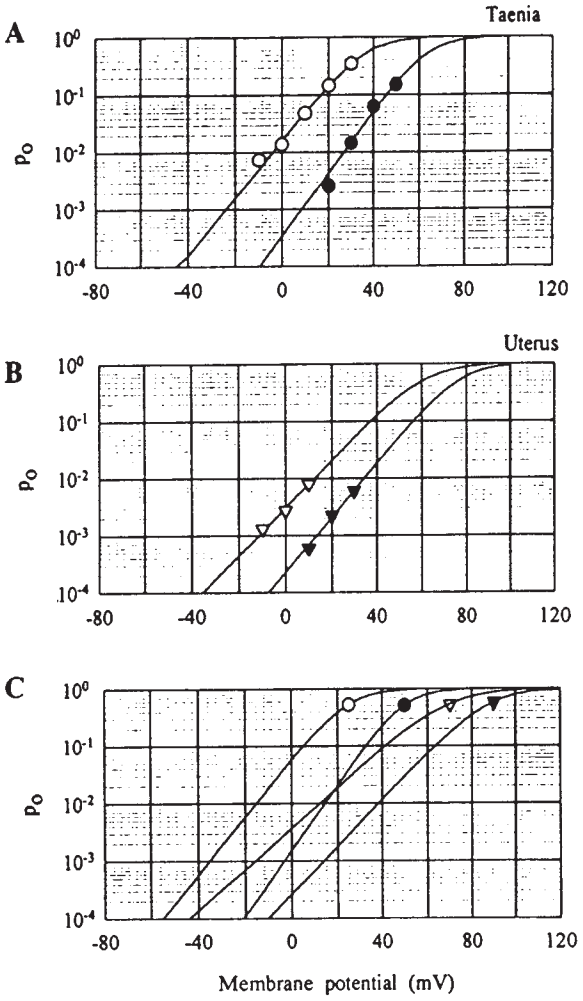

FIGURE 14. Voltage–open probability relations of maxi-K channels from *taenia coli* myocyte and late-pregnant uterine myocyte, and effects of $[Ca^{2+}]_i$ on them. (*A* and *B*) Data from representative individual patch for illustration. (*C*) Summary of data. In *A* and *B*, solid curves are Boltzmann distributions: $P_o = [1 + \exp(V_h - V)/k]^{-1}$, where V_h is voltage at which $P_o = 0.5$, and k is logarithmic voltage sensitivity. Filled symbols for pCa 8; hollow symbols for pCa 7. (*A*) For *taenia coli* channel, V_h and k are, respectively, 63.2 and 7.9 mV for pCa 8, and 35.4 and 8.9 mV for pCa 7. (*B*) For late-pregnant myometrial channels, they are, respectively, 76.3 and 9.1 mV for pCa 8, and 60.3 and 10.4 mV for pCa 7. Differences: in myometrial channel, V_h is more positive, k is shallower, and negative shift of V_h on increasing $[Ca^{2+}]_i$ is less. (*C*) Average P_o-V relations of late-pregnant maxi-K channel compared with those of *taenia coli* channel. Curves are computed Boltzmann distributions based on mean data of V_h and k obtained individually from six *taenia coli* patches and nine myometrial patches. Each curve is identified by average V_h value used; triangles for myometrial channels, circles for *taenia coli* channels. Filled symbols for pCa 8, hollow symbols for pCa 7. See text for data.

DISCUSSION

Confusion abounds in our knowledge of myometrial K^+ currents, possibly because of concurrent expressions of multiple types of channels and labile combinations of channel types engendered by hormonal influences. Previous studies centered on single states of the myometrium (Mironneau and Savineau, 1980; Miyoshi et al., 1991; Piedras-Renteria et al., 1991; Inoue et al., 1993), or identified tissue-cultured material with freshly dissociated myocytes (Toro et al., 1990; Erulkar et al., 1994). As whole-cell K^+ currents were generally treated in their entirety, variance could be expected between extant claims and the present results. Thus, the prominence of a Ca^{2+}-activated K^+ current in multicellular preparations of late-pregnant myometrium (Mironneau and Savineau, 1989) is inconsistent with the Ca^{2+} insensitivity of myocytes from such preparations (Figs. 2 and 3; also Kao et al., 1989; Miyoshi et al., 1991; Inoue et al., 1993). A transient outward current in late-pregnant myocytes surmised solely on the basis of 4-AP action (Inoue et al., 1993) may have resulted from an unobserved slowing of activation of I_K by 4-AP (see Fig. 11, *F* and *G*), because such a current was not seen in late-pregnant myocytes. The difficulties of equating tissue-culture material with freshly dissociated myocytes is exemplified by the fact that three K^+ currents in freshly dissociated nonpregnant myocytes (Piedras-Renteria et al., 1991) were very different from those seen by the same investigators in tissue-cultured material (Toro et al., 1990). They also lack counterparts in the present study, not least because they could not be recorded with pipette solutions containing Ca^{2+} buffers (contrast also Miyoshi et al., 1991). The I_{TO} of the present study, half inactivated at −77 mV and half activated at 5 mV (Fig. 6 *A*) is clearly different from an incompletely characterized transient K^+-current (K_t) that was half activated at 22 mV (Piedras-Renteria et al., 1991), and another seen in tissue-cultured material that was half inactivated at −48 mV (Erulkar et al., 1994).

Although the whole-cell approach used in this study cannot identify native K^+ channels with cloned K^+ channels (because of accessory unit influence or heteromultimeric assembly), the paradigm used has sorted out more concurrent K^+ currents in smooth myocytes than had been accomplished before. The combined sifting with holding potentials and blocking agents also recognized the appropriate roles of some channels that would have been masked in a whole-cell current approach. In uterine myocytes, the K^+ currents are due to voltage-gated (K_v) currents and their related Ca^{2+}-activated K^+ (K_{Ca}) currents. No inwardly rectifying K^+ currents were detected.

By their noninactivating nature, noisiness and susceptibility to IbTX (Fig. 10 *G*), 85–90% of the C_3 currents are attributed to large-conductance K_{Ca} channels, a surmise consistent with their nonresponsiveness to 4-AP. The C_2 currents contained several types of K_{Ca} currents and K_v currents: K_{Ca} currents of the small- or intermediate-conductance varieties were recognized by their susceptibility to ChTX and apamin, and K_v currents by their suscepti-

bility to 4-AP, DTX, and MCDP. The C_1 currents contained the most diverse constituents of both K_v and K_{Ca} types. Of the K_v currents, because of vast differences in their steady state gating properties (Fig. 6), the I_{TO} and the delayed-rectifier currents probably originated in different channels rather than in a single channel type with different accessory-unit modification of their inactivation kinetics. That 4-AP had no preferential effect on the I_{TO} suggested that the native I_{TO} channel(s) might be closer to rK_v 1.4 than to rK_v 3.3 or rK_v 3.4 (see Chandy and Gutman, 1995). In late-pregnant myocytes, the gating and pharmacological properties of the native K^+ channels resembled those of cloned rK_v 1.1, 1.2, 1.6 channels (see Chandy and Gutman, 1995).

Changes in Myometrial K^+ Currents During Pregnancy

Among many similarities in the K^+ currents of nonpregnant and late-pregnant myocytes, three differences are particularly notable: (*a*) I_{TO}, often present in nonpregnant myocytes, is absent in late-pregnant myocytes; (*b*) K^+ currents of late-pregnant myocytes are insensitive or much less sensitive than those of nonpregnant myocytes to changes in intracellular or extracellular Ca^{2+}; and (*c*) some delayed-rectifier currents are seen only in late-pregnant myocytes.

As I_{TO} regulates the membrane potential during burst spike discharges (Conner and Stevens, 1971), its absence in late pregnancy removes a constraint on repetitive action potentials that occur with greater frequencies as term approaches. Several factors underlie the relative Ca^{2+} insensitivity of late-pregnant myocytes. Firstly, there are differences in screenable surface negative charges (Frankenhauser and Hodgkin, 1957), whereas voltage-activation relations of nonpregnant myocytes were shifted 15 mV to the positive by elevated $[Ca^{2+}]_o$, those of late-pregnant myocytes were unaffected (Fig. 7). Such a charge-screening effect must also influence the voltage-inactivation relations. Thus, for nonpregnant myocytes held at −50 mV, a 15-mV shift would increase the available fraction of I_{TO} from ~1% in 1 mM Ca^{2+} (Fig. 6 *A*) to ~20% in 30 mM Ca^{2+}, enough to largely account for a revival of an I_{TO} that had been inactivated (Fig. 2). Other factors involve more direct changes in K^+ channel types. Pharmacological responses indicate that as pregnancy progressed towards term, maxi-K (K_{Ca}) channels are replaced by smaller-conductance delayed rectifier (K_v) channels to express whole-cell K^+ currents. This change accounts for the difference between the noisy and outwardly rectifying current of nonpregnant myocytes and the rather smooth current with little rectification of the late-pregnant myocytes.

The lowered expression of maxi-K channels can result from a reduced density and/or altered conditions for their expression. A reduced density is suggested by the different responses of the I_K of nonpregnant and of late-pregnant myocytes to photolysis-induced increase of $[Ca^{2+}]_i$ (Fig. 4). The possibility of altered conditions of expression is shown in the V-*g* relations of the C_3 currents (Fig. 6 *D*; 39 mV for nonpregnant myocytes and 63 mV for late-pregnant myocytes), which are mostly due to IbTX-sensitive large-conductance K_{Ca} channel(s) (Fig. 10 *G*). Single maxi-K channels from late-pregnant myocytes have a half-open probability in pCa 7 of 68 mV (Fig. 14). They are also less sensitive to Ca^{2+} than similar channels in *taenia coli* myocytes, which express them abundantly. Limiting the expression of maxi-K channels could increase myometrial excitability by setting the resting potential positive to the potassium equilibrium potential, and by decreasing the resting membrane conductance and thereby lowering the current needed to trigger action potentials. Fig. 6 *D* shows that, in the physiological range of voltages, differences in the fractional activation of these currents are substantial. For instance, at −20 mV (near the spike threshold), the fractional activation is 0.03 for nonpregnant myocytes and 0.005 for late-pregnant myocytes; at 20 mV (near the peak of action potentials), these fractions are 0.26 and 0.08, respectively.

In conclusion, as pregnancy progresses towards term, myometrial maxi-K channels lose functional importance through a combination of factors that include a change in surface negative charges, a reduction in density, a positive shift of voltage-activation relation, and a lowered sensitivity to Ca^{2+}. In concert with a suppression of I_{TO} and an increased expression of a fast Na^+ channel (Yoshino et al., 1997), these changes facilitate repetitive spike discharges for the needs of parturition.

This paper is dedicated to Chien Yuan Kao, M.D., who died unexpectedly on May 26, 1998. My father introduced me to scientific research and medicine and served as my most trusted mentor and closest friend throughout my life (P.N. Kao). The C.Y. Kao Memorial Medical Student Research Scholarship Fund has been established to support training in basic science investigation, and is administered at the Department of Pharmacology, State University of New York Health Sciences Center.

The work described was supported by grants from the National Institutes of Health (HD00378 and DK39371).

Original version received 18 June 1998 and accepted version received 21 September 1998.

REFERENCES

Amman, D. 1986. Ion Selective Microelectrodes. Springer Verlag GmbH & Co. Berlin, Germany. 109–207.

Blatz, A.L., and K.L. Magleby. 1986. Single apamine-blocked Ca^{2+}-activated K^+ channels of small conductance in cultured rat skeletal muscle. *Nature.* 323:718–720.

Brau, M.E., F. Dreyer, P. Jones, H. Repp, and W. Vogel. 1990. A K^+ channel in *Xenopus* nerve fibers selectively blocked by bee and snake toxins: binding and voltage-clamp experiments. *J. Physiol. (Camb.).* 420:365–385.

Chandy, K.G., and G.A. Gutman. 1995. Voltage-gated potassium channel genes. *In* Handbook of Receptors and Channels, Ligand and Voltage-Gated Ion Channels. R.A. North, editor. CRC Press. Boca Raton, FL. 1–71.

Conner, J.A., and C.F. Stevens. 1971. Voltage clamp studies of a transient outward membrane current in gastropod neural somata. *J. Physiol. (Camb.).* 213:21–30.

Dreyer, F. 1990. Peptide toxins and potassium channels. *Rev. Physiol. Biochem. Pharmacol.* 115:93–136.

Erulkar, S.D., J. Rendt, R.D. Nori, and B. Ger. 1994. The influence of 17-oestradiol on K^+ currents in smooth muscle cells isolated from immature rat uterus. *Proc. R. Soc. Lond. B Biol. Sci.* 256:59–65.

Fan, S.F., S.Y. Wang, and C.Y. Kao. 1993. The transduction pathway of isoproterenol activation of the Ca^{2+}-activated K^+ channel in guinea pig *taenia coli* myocyte. *J. Gen. Physiol.* 102:257–275.

Frankenhauser, B., and A.L. Hodgkin. 1957. The role of calcium on the electrical properties of squid axon. *J. Physiol. (Camb.).* 137: 218–244.

Galvez, A., G. Gimenez-Gallego, J.P. Reuben, L. Roy-Contacin, P. Feigenbaum, G.J. Kaczorowski, and M.L. Garcia. 1990. Purification and characterization of a unique potent peptidyl probe for the high conductance calcium-activated potassium channel from venom of the scorpion *Buthus tamulus. J. Biol. Chem.* 265:11083–11090.

Garcia, M.L., H.G. Knaus, P. Munujos, R.S. Slaughter, and G.J. Kaczorowski. 1995. Charybdotoxin and its effects on potassium channels. *Am. J. Physiol.* 269:C1–C10.

Gurney, A.M., R.Y. Tsien, and H.A. Lester. 1987. Activation of a potassium current by rapid photochemically generated step increase of intracellular calcium in rat sympathetic neurons. *Proc. Natl. Acad. Sci. USA.* 84:3496–3500.

Hille, B. 1992. Ionic Channels of Excitable Membranes. 2nd ed. Sinauer Associates, Inc. Sunderland, MA. p. 115.

Hu, S.L., Y. Yamamoto, and C.Y. Kao. 1989*a*. The Ca^{2+}-activated K^+ channel and its functional roles in smooth muscle cells of the guinea pig *taenia coli. J. Gen. Physiol.* 94:833–847.

Hu, S.L., Y. Yamamoto, and C.Y. Kao. 1989*b*. Permeation, selectivity, and blockade of the Ca^{2+}-activated potassium channel of the guinea pig *taenia coli* myocyte. *J. Gen. Physiol.* 94:849–862.

Inoue, Y., K. Shimamura, and N. Sperelakis. 1993. Forskolin inhibition of K^+ current in pregnant rat uterine smooth muscle cells. *Eur. J. Pharmacol.* 240:169–176.

Jan, L.Y., and Y.N. Jan. 1997. Cloned potassium channels from eukaryotes and prokaryotes. *Annu. Rev. Neurosci.* 20:91–123.

Kao, C.Y., and J.R. McCullough. 1975. Ionic currents in the uterine smooth muscle. *J. Physiol. (Camb.).* 246:1–36.

Kao, C.Y., and M.J. Siegman. 1963. Nature of electrolyte exchange in isolated uterine smooth muscle. *Am. J. Physiol.* 205:674–680.

Kao, C.Y., M. Wakui, S.Y. Wang, and M. Yoshino. 1989. The outward current of the isolated rat myometrium. *J. Physiol. (Camb.).* 418:20.

Kaplan, J.H. 1990. Photochemical manipulation of divalent cation levels. *Annu. Rev. Physiol.* 52:897–914.

Miller, C., E. Moczydlowski, R. Lattore, and M. Philippa. 1985. Charybdotoxin, a potent inhibitor of single Ca^{2+}-activated K^+ channels from mammalian skeletal muscle. *Nature.* 313:316–318.

Mironneau, J., and J.P. Savineau. 1980. Effects of calcium ions on outward membrane currents in rat uterine smooth muscle. *J. Physiol. (Camb.).* 302:411–425.

Miyoshi, H., T. Urabe, and A. Fujiwara. 1991. Electrophysiological properties of membrane currents in single myometrial cells isolated from pregnant rats. *Pflügers Arch.* 419:386–393.

Parkington, H.C., and H.A. Coleman. 1990. The role of membrane potential in the control of uterine activity. *In* Uterine Function. M.E. Carsten and J. Miller, editors. Plenum Publishing Corp. New York. p. 219.

Piedras-Renteria, E., L. Toro, and E. Stefani. 1991. Potassium currents in freshly dispersed myometrial cells. *Am. J. Physiol.* 251: C278–C284.

Romey, G., M. Hugues, H. Schmid-Antonmarchi, and M. Lazdunski. 1984. Apamin: a specific toxin to study a class of Ca^{2+}-activated K^+ channels. *J. Physiol. (Paris).* 79:259–264.

Suput, D., M. Yoshino, S.Y. Wang, and C.Y. Kao. 1989. Ionic currents in freshly dissociated rat myometrial cells. *FASEB J.* 3:*A*254.

Stansfeld, C.E., S.J. Marsh, D.M. Parcej, J.O. Dolly, and D.A. Brown. 1987. Mast cell degranulating peptide and dendrotoxin selectively inhibit a fast-activating potassium current and bind to common neuronal proteins. *Neuroscience.* 23:893–902.

Sui, J.L., and C.Y. Kao. 1997. Role of outward potassium currents in the action potential of guinea pig ureteral myocytes. *Am. J. Physiol.* 273:C962–C972.

Toro, L., E. Stefani, and S. Erulkar. 1990. Hormonal regulation of potassium currents in single myometrial cells. *Proc. Natl. Acad. Sci. USA.* 87:2892–2895.

Vasquez, J., P. Feigenbaum, G.M. Katz, V.F. King, J.P. Reuben, L. Roy-Contancin, R.S. Slaughter, G.J. Kaczorowski, and M.L. Garcia. 1989. Characterization of high-affinity binding sites for charybdotoxin in sarcolemmal membranes from bovine aortic smooth muscle. *J. Biol. Chem.* 264:20902–20909.

Wang, S.Y., M. Yoshino, J.L. Sui, and C.Y. Kao. 1996. Pregnancy and K^+ currents of freshly dissociated rat uterine myocytes. *Biophys. J.* 70:*A*396.

Yamamoto, Y., S.L. Hu, and C.Y. Kao. 1989. Outward current in single smooth muscle cells of the guinea pig *taenia coli. J. Gen. Physiol.* 93:551–564.

Yoshino, M., S.Y. Wang, and C.Y. Kao. 1989. Ionic currents in smooth myocytes of the pregnant rat uterus. *J. Gen. Physiol.* 94:38*a*.

Yoshino, M., S.Y. Wang, and C.Y. Kao. 1997. Sodium and calcium inward current in freshly dissociated smooth myocytes of rat uterus. *J. Gen. Physiol.* 110:565–577.